Journal of Marine Research, 59, 133–166, 2001

Absorbed Mn^{2+} and Mn redox cycling in Iberian continental margin sediments (northeast Atlantic Ocean)

by Claar van der Zee[1], Wim van Raaphorst[1] and Eric Epping[1]

ABSTRACT

Although Mn^{2+} sorption has been investigated extensively in the laboratory, the role of Mn^{2+} sorption in natural marine sediments remains speculative. Our objectives were to study (1) the role of Mn^{2+} sorption in the redox cycling of Mn, (2) to quantify Mn cycling and (3) to identify its rate-determining factors at the Iberian margin.

Profiles of pore water Mn^{2+}, adsorbed Mn^{2+} and solid phase Mn were measured together with benthic oxygen fluxes along three transects across the margin from the shelf to the deep sea as well as in the Nazeré Canyon. In the profiles, peaks of adsorbed Mn^{2+} were observed in-between those of solid phase Mn and pore water Mn^{2+}. We propose that upon Mn reduction, the produced Mn^{2+} is adsorbed onto adjacent Mn oxide or oxyhydroxide surfaces. Available adsorption-sites diminish and/or saturate as Mn reduction continues, upon which Mn^{2+} is released into the pore water. Mn redox chemistry is controlled by the organic carbon flux to the sediment. A simple steady state model was formulated that includes Mn^{2+} sorption as a combination of an instantaneous reversible equilibrium process and a first-order kinetic reaction. Model derived, depth integrated rates of Mn reduction as well as Mn^{2+} desorption and oxidation rates range between 1 and 35 μmoles m^{-2} d^{-1}. Mn cycling is most intense at moderate carbon fluxes. Moreover, Mn cycling is enhanced at higher deposition fluxes of Mn oxide in the canyon. Budgets based on the model indicate that adsorbed Mn^{2+} is an important redox intermediate between Mn oxide and pore water Mn^{2+} in the reduced sediment layer. Adsorption of Mn^{2+} restrains the efflux of dissolved Mn^{2+} into the water column, by lowering the pore water gradient at stations with a thin oxidation zone. There, adsorbed Mn^{2+} enhances the retention of Mn^{2+} in the sediment column.

1. Introduction

Mn can be the most important intermediate oxidant between oxygen and organic carbon in marine sediments (Aller, 1990, 1994; Canfield *et al.,* 1993; Thamdrup *et al.,* 1994). Coupled to the oxidation of organic matter is the reduction of a suite of electron acceptors, e.g., oxygen, nitrate, manganese and iron (hydr-) oxides and sulphate (Froelich *et al.,* 1979). Depending on the carbon flux to the sediment, sedimentation rate and sediment mixing intensity, these electron acceptors each contribute to a different extent to the oxidation of organic carbon. At low carbon fluxes, oxygen is the most important electron acceptor (Bender and Heggie, 1984) whereas sulphate reduction is most important at high

1. Department of Marine Chemistry and Geology, Netherlands Institute for Sea Research, P.O. Box 59, 1790 AB Den Burg, The Netherlands. ***email: claarz@nioz.nl***

carbon fluxes (Jørgensen, 1982). The relative contribution of Mn reduction to the oxidation of organic matter is largest at moderate carbon fluxes when oxygen is depleted within a few cm (Aller, 1990). Mn^{2+} is produced upon Mn-oxide reduction, which is either directly coupled to organic carbon oxidation (Myers and Nealson, 1988a) or via the oxidation of reduced solutes like Fe^{2+}, sulphide or organic acids (Myers and Nealson, 1988b; Stone, 1987).

Adsorption of Mn^{2+} is an important step prior to both its oxidation as well as the precipitation of (Ca,Mn)-CO_3 (Franklin and Morse, 1983; Wilson, 1980). Surfaces appear to bind Mn^{2+} in a manner that facilitates the transition state necessary for oxidation (Wilson, 1980). In a classical experiment, Morgan and Stumm (1964) found that the adsorption capacity at pH 7.5 was as much as 0.5 mole Mn^{2+} per mole MnO_2. While many laboratory investigations have studied Mn^{2+} sorption (Morgan and Stumm, 1964; Murray, 1975; Wilson, 1980; Franklin and Morse, 1983; Davies and Morgan, 1989; Burdige *et al.,* 1992; Fendorf *et al.,* 1993; Junta and Hochella, 1994; Junta-Rosso *et al.,* 1997), little attention has been paid to the role of Mn^{2+} sorption in natural marine sediments. Van Cappellen and Wang (1996) explicitly included the adsorption reaction of Mn^{2+} as a complexation reaction with hydrated surface sites in their diagenetic model. However, in most diagenetic models, adsorption of Mn^{2+} is either neglected (Burdige and Gieskes, 1983; Dhakar and Burdige, 1996; Van Cappellen and Wang, 1995) or instantaneous reversible equilibrium with pore water Mn^{2+} is assumed, using a sorption constant from the literature (Slomp *et al.,* 1997; Aller, 1994). Sorption constants were derived experimentally in a few studies only, e.g., for a Danish coastal sediment (Canfield *et al.,* 1993), for Mn oxides (Burdige *et al.,* 1992), for kaolinite and a mixture of kaolinite with calcite (Burdige and Kepkay, 1983). Canfield *et al.* (1993) noted a pronounced difference in the adsorption capacity of Mn^{2+} onto sediments containing fully oxidized Mn and sediment with Mn oxides having an average oxidation level less than 3.6–3.8. Furthermore, they found that adsorption of Mn^{2+} onto natural sediments was not completely reversible.

In this paper we present data on the vertical distribution of adsorbed Mn^{2+}, pore water Mn^{2+}, and solid phase Mn in sediments from the Iberian continental margin. A simple reaction-diffusion model was formulated in order to estimate depth-integrated rates of Mn reduction, Mn^{2+} desorption and oxidation, as well as to assess the consistency of the distribution of the three Mn phases. In addition, carbon oxidation rates were determined since Mn reduction rates may vary with the amount and degradability of the carbon flux to the sediment. Thus, the following objectives are addressed (1) the role of Mn^{2+} sorption in the Mn redox cycle, (2) quantification of the Mn redox cycle and (3) the identification of its rate-determining factors.

2. Research area

Our research area comprised the Iberian continental margin in the northeastern Atlantic (Fig. 1). The stations were visited during two cruises with R.V. *Pelagia* within the Ocean Margin Exchange Project (OMEX II) in August 1998 and May 1999 (Table 1). Sediments

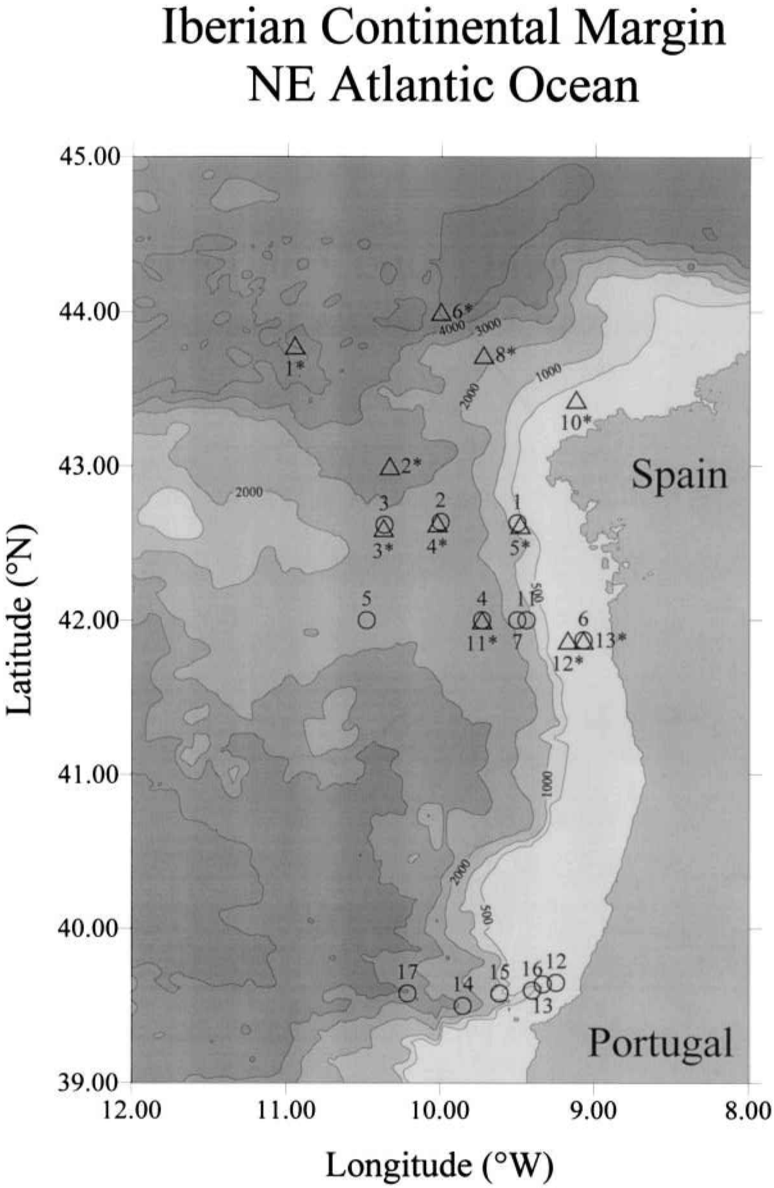

Figure 1. Map of the Iberian Margin indicating positions of sampled stations in 1998 (triangles, numbers with asterisk) and 1999 (circles, numbers without asterisk).

are clastic with a minor biogenic component. Sediment transport and accumulation is described in detail by Van Weering *et al.* (2001). Particles are transported from the shelf in benthic nepheloid layers, forming intermediate nepheloid layers at the shelf break. Main deposition occurs within 50 km off shore. Organic carbon contents vary between 0.33 and

Table 1. Name, water depth, geographical position, bottom water (BW) temperature and oxygen concentration and organic carbon content of the visited stations, number 121-stations are visited in August 1998 and number 138-stations are visited in May 1999.

Station	Water depth (m)	Lat. °N	Long. °W	BW Temp (°C)	BW O_2 (μM)	Corg* (wt %)
I La Coruña Transect						
121-10	175	43.26	09.07	12.1	225	0.33
121-08	2109	43.43	09.43	3.2	250	1.04
121-06	4908	44.00	10.00	3.1	245	0.72
121-01	4941	43.47	10.57	3.1	245	0.45
II Vigo Transect						
138-01	213	42.38	09.28	12.1	213	0.47
121-05	223	42.38	09.29	12.0	223	0.62
138-02	2164	42.38	10.00	3.4	249	1.35
121-04	2213	42.38	10.01	3.2	250	1.16
138-03	2932	42.37	10.22	2.5	243	1.01
121-03	2926	42.36	10.22	3.1	243	0.87
121-02	3371	43.00	10.20	3.1	245	1.08
III Main Transect						
121-13	104	41.52	09.04	12	235	4.58
138-06	113	41.52	09.04	12.5	210	4.46
121-12	123	41.52	09.10	12.1	230	0.42
138-11	932	42.00	09.26	—	—	1.41
138-07	1387	42.00	09.28	10.3	188	1.99
138-04	2060	42.00	09.44	3.8	247	1.17
121-11	2073	42.00	09.44	3.4	255	1.41
138-05	2853	42.00	10.30	2.6	241	0.88
IV Nazaré Canyon Transect						
138-13	137	39.39	09.20	12.8	209	0.86
138-12	344	39.39	09.15	12.2	206	3.46
138-15	396	39.35	09.37	11.6	200	1.04
138-16	890	39.36	09.24	11.0	189	3.12
138-14	3097	39.31	09.51	2.4	243	3.67
138-17	4280	39.35	10.17	2.1	243	2.56

*Organic carbon content in 0–2.5 mm interval.

4.58 wt% C in the upper sediment layer (Table 1). In general, median grain sizes decrease with increasing distance to the shore, however, some local organic-rich muds are found near the shelf edge. The relative contribution of three grain size fractions to the bulk sediment composition is given in Figure 2.

Different depositional areas were sampled along three transects from the shelf across the margin to the deep sea and one transect in the Nazaré Canyon. As other submarine canyons (Durrieu de Madron *et al.,* 1999; Monaco *et al.,* 1999; Sanchez-Cabeza *et al.,* 1999) the Nazaré Canyon is a preferential transport route for particulate material from the shelf to the

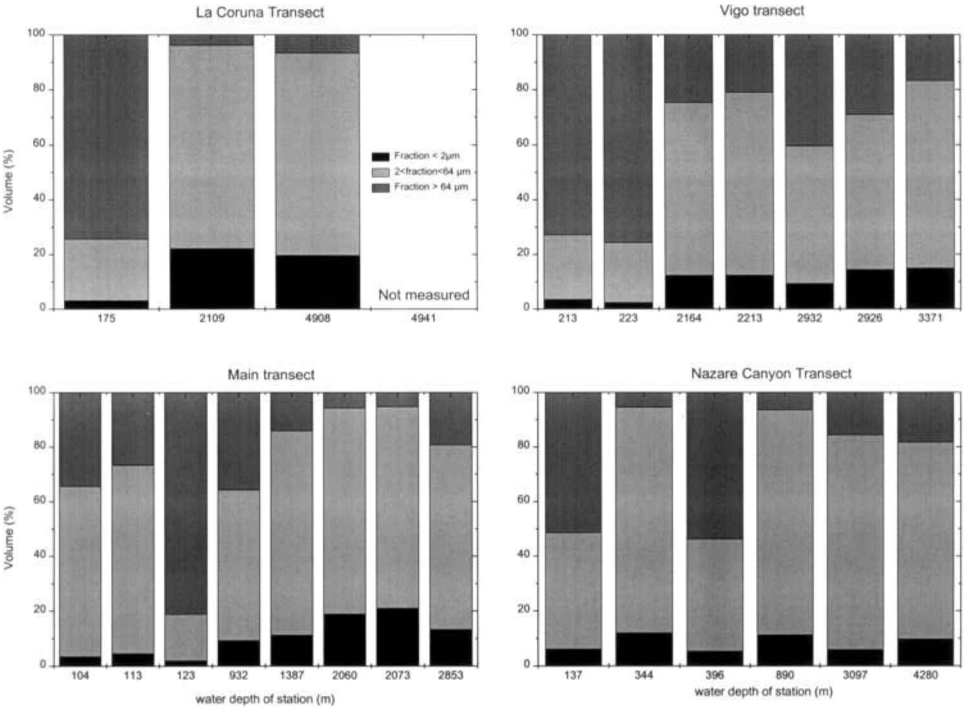

Figure 2. Relative contributions of three grain size fractions to the sediment composition of the upper sediment layer.

deep sea (Epping *et al.,* 2001; Van Weering *et al.,* 2001). The northern most La Coruña transect is characterized by a gradual decreasing water depth, whereas the slope is steeper at both the Vigo transect north of Vigo, and the main transect south of Vigo. The fourth transect is in the Nazaré Canyon farther to the south. There, four stations were sampled and an additional two on the adjacent shelf.

3. Material and methods

Sediment cores were taken with a multi-corer and processed at *in situ* temperature directly upon retrieval. Four sediment cores were sliced simultaneously for pore water collection with a hydraulic core-slicer developed at NIOZ to obtain high spatial resolution at the sediment-water interface. The slicer electronically logs the vertical position of the extruder pistons with an accuracy of <0.1 mm, relative to the sediment-water interface. The sediment was sectioned in 2.5-mm slices in the upper 10 mm of the sediment, in 5-mm slices from 10 to 30 mm, in 10-mm slices from 30 to 60 mm and in 20-mm slices farther down. Slices from corresponding depth intervals were pooled and centrifuged (3000 rpm, 10 min) for pore water extrusion. Depth intervals were pooled to increase the volume of pore water for analysis of several other pore water constituents required in the OMEX

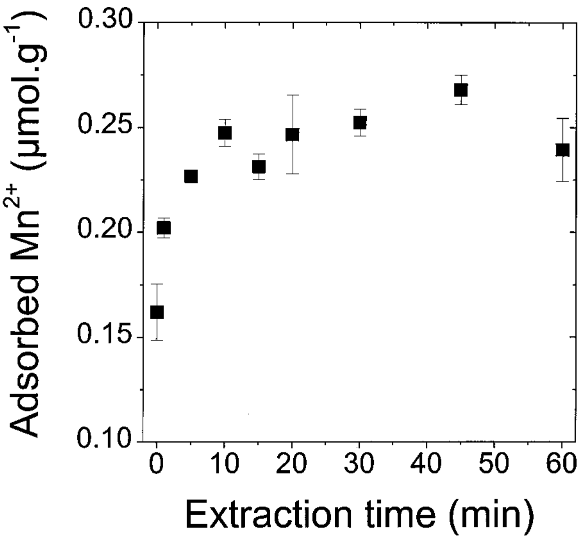

Figure 3. Amount of Mn extracted with 50 mM $CuSO_4$ as a function of incubation time. Each data point is the average of three measurements.

project and might have led to some of the scatter in the profiles. Pore water was filtered (0.45 μm, Acrodisc) and analyzed shipboard for nitrate and manganese on a TRAACS-800 auto-analyzer. Nitrate was analyzed according to Strickland and Parsons (1972). Aliquots for manganese were acidified to pH 2 and analyzed according to the method of Brewer and Spencer (1971). After pore water collection the centrifuged sediment was stored frozen (−20°C) until further analysis for solid phase manganese at the NIOZ laboratory. Adsorbed Mn^{2+} was determined using a $CuSO_4$ sediment extraction (Bromfield and David, 1976; Lovley and Phillips, 1988). The principle of the extraction method is the exchange of Mn^{2+} by Cu^{2+} (Bromfield and David, 1976). It is assumed that the total dissolved Mn was reduced since 2+ is the dominant valence for dissolved Mn in seawater (Bruland, 1983). To test the optimal incubation time for the $CuSO_4$ extraction, sediment samples were incubated in triplo with 50 mM $CuSO_4$ for 0, 1, 5, 10, 15, 20, 30, 45 and 60 min. The amount of extracted Mn did not further increase upon incubation longer than 20 min (Fig. 3). Thawed sediment from the 1998 cruise was extracted with 50 mM $CuSO_4$ for 20 min in the laboratory. During the 1999 cruise an additional core was sliced and wet sediment was extracted with 50 mM $CuSO_4$ for 20 min directly onboard. The extract was filtered (0.45 μm, Acrodisc), acidified and stored cool (4°C) and in the dark. Corrections were made for the pore water Mn^{2+} in the extract. Freeze-dried and ground sediment was extracted with 1N HCl (24 hrs, 20°C) for solid phase Mn, which includes reactive Mn-oxides and Mn-carbonates (Thamdrup *et al.,* 1994; Slomp *et al.,* 1997). Mn both in the $CuSO_4$ and the HCl extracts was measured by flame AAS. Porosity was determined from the weight loss of the sediment after drying at 60°C and assuming a specific weight of the sediment particles of 2.65 g cm^{-3}. Oxygen fluxes were estimated from microprofiles measured *in situ* with Clark-type oxygen microelectrodes mounted on a benthic profiling lander (TROL), or were estimated by modeling the nitrate, ammonium, and sediment organic carbon profile using a numerical, coupled diagenetic model (OMEXDIA) (Soetaert *et al.,* 1996). Further details are described in Epping *et al.* (2001).

4. The model

a. Description

Early diagenetic models have been developed that couple the diagenesis of Mn to the cycles of C, N, O, P, S and Fe (Rabouille and Gaillard, 1991; Dhakar and Burdige, 1996; Van Cappellen and Wang, 1996; Boudreau *et al.,* 1998). None of these models, however, includes a kinetic sorption reaction for Mn^{2+}. In case instantaneous equilibrium sorption with a depth invariant isotherm dominates, adsorbed and pore water Mn^{2+} have parallel profiles with peaks in the same depth interval (Berner, 1976). Our profiles show that adsorbed Mn^{2+} accumulates at shallower depths in the sediment than dissolved Mn^{2+}, indicating that instantaneous equilibrium sorption was not the only sorption process. Therefore, we developed a new, but simpler model than the coupled models mentioned above. This allowed us to reduce the number of variables, limit the uncertainties in data of other elements that could affect the modeling of Mn, and to focus on the role of sorption in the redox cycle of Mn.

Our model is similar to the Mn model of Slomp *et al.* (1997) with additional kinetic sorption. Compared to their model, the uncertainty associated with the kinetic parameters is compensated for by the extra data provided by the adsorbed Mn^{2+} profiles. A listing of all model parameters is given in Table 2. In the model the molecular sediment diffusion coefficient (*Ds*), bioturbation coefficient (*Db*), all reaction rate constants, the instantaneous equilibrium sorption coefficient (K_{eq}) and sediment porosity are assumed to be depth-independent for simplicity sake. Also, the sedimentation rate (ω) is assumed to be constant, which is likely for the deep-sea stations, but for the slope and shelf stations sedimentation is probably more pulsed on a seasonal scale. However, sedimentation rates are not affected by seasonal variation and our profiles do not indicate that pulsed sedimentation had occurred shortly prior to sampling. The model is a one-dimensional steady-state reaction-diffusion model that includes Mn^{2+} sorption as a combination of an instantaneous reversible equilibrium process and a first-order kinetic reaction. The sediment was divided into an oxidized and a reduced layer. The redox boundary at depth L is given by the maximum depth of oxygen penetration if known or the inflection point in the nitrate profile otherwise (Aller, 1994; Slomp *et al.,* 1997).

In the oxidized layer, Mn^{2+} is both oxidized and adsorbed. Oxidation of dissolved and adsorbed Mn^{2+} is described as first-order processes with k_{oxc} and k_{oxa} as the oxidation rate constants, respectively. Kinetic adsorption is described as a first-order process with k_{ads} as the adsorption rate constant. The dimensionless sorption coefficient for equilibrium sorption (K_{eq}) is set at 1 (Slomp *et al.,* 1997) and C_{eq} is the pore water equilibrium concentration. For the conversion between pore water and solid phase Mn or adsorbed

Table 2. Name, unit and function of model parameters.

Name	Unit	Function
Ds	$m^2\ d^{-1}$	Molecular sediment diffusion coefficient
Db	$m^2\ d^{-1}$	Bioturbation coefficient
ω	$m\ d^{-1}$	Sedimentation rate
x	m	Depth in sediment
L	m	Depth of Mn redox boundary
K_{eq}	—	Dimensionless sorption coefficient for equilibrium sorption
C_{eq}	$mol\ m^{-3}$	Pore water equilibrium concentration
ϕ	—	Sediment porosity
ρ	$g\ cm^{-3}$	Average density of the sediment
ϑ	$g\ cm^{-3}$	Conversion factor between pore water and solid or adsorbed phase
C_I	$mol\ m^{-3}$	Pore water Mn^{2+} concentration in the oxidized layer
C_{II}	$mol\ m^{-3}$	Pore water Mn^{2+} concentration in the reduced layer
A_I	$\mu mol\ g^{-1}$	Adsorbed Mn^{2+} concentration in the oxidized layer
A_{II}	$\mu mol\ g^{-1}$	Adsorbed Mn^{2+} concentration in the reduced layer
S_I	$\mu mol\ g^{-1}$	Solid phase Mn concentration in the oxidized layer
S_{II}	$\mu mol\ g^{-1}$	Solid phase Mn concentration in the reduced layer
C_a	$mol\ m^{-3}$	Pore water equilibrium concentration for precipitation
A_{eq}	$\mu mol\ g^{-1}$	Adsorbed Mn^{2+} concentration at which no further reactions occur
S_{eq}	$\mu mol\ g^{-1}$	Solid phase Mn concentration at which no further reactions occur
k_{oxc}	d^{-1}	Dissolved Mn^{2+} oxidation rate constant
k_{oxa}	d^{-1}	Adsorbed Mn^{2+} oxidation rate constant
k_{ads}	d^{-1}	Adsorption rate constant
k_r	d^{-1}	Reduction rate constant
k_{des}	d^{-1}	Desorption rate constant
k_a	d^{-1}	Precipitation rate constant
$J_{Sx=0}$	$\mu mol\ m^{-2}\ d^{-1}$	Flux of solid phase Mn at the sediment-water interface
$J_{Ax=0}$	$\mu mol\ m^{-2}\ d^{-1}$	Flux of adsorbed Mn^{2+} at the sediment-water interface

Mn^{2+} the factor ϑ (gram of dry sediment per cm^3 of pore water) is used: $\vartheta = \rho[(1 - \phi)/\phi]$, where ρ is the average density of the sediment (2.65 g cm^{-3}) and ϕ is sediment porosity. Differential equations for dissolved Mn^{2+} (C_I), adsorbed Mn^{2+} (A_I), and solid phase Mn (S_I) in the oxidized layer as a function of depth in the sediment (x) are:

$$[(1 + K_{eq})Db + Ds]\frac{\delta^2 C_I}{\delta x^2} - (1 + K_{eq})\omega\frac{\delta C_I}{\delta x} - k_{oxc}C_I - k_{ads}(C_I - C_{eq}) = 0 \qquad (1)$$

$$Db\frac{\delta^2 A_I}{\delta x^2} - \omega\frac{\delta A_I}{\delta x} - k_{oxa}A_I + \frac{k_{ads}}{\vartheta}(C_I - C_{eq}) = 0 \qquad (2)$$

$$Db\frac{\delta^2 S_I}{\delta x^2} - \omega\frac{\delta S_I}{\delta x} + k_{oxa}A_I + \frac{k_{oxc}}{\vartheta}C_I = 0 \qquad (3)$$

In the reduced layer, Mn reduction, Mn^{2+} desorption and precipitation occur. Dissolved Mn^{2+} production due to desorption is described as a first-order process with k_{des} as desorption rate constant. Removal of Mn^{2+} due to authigenic mineral formation is described as a first-order process with k_a as the precipitation rate constant. Production of adsorbed Mn^{2+} due to solid phase Mn reduction is described as a first-order process with k_r as the reduction rate constant. The pore water equilibrium concentration for precipitation is C_a. The concentrations for adsorbed Mn^{2+} and solid phase Mn at which no further reactions occur are A_{eq} and S_{eq}, respectively. Differential equations for dissolved Mn^{2+} (C_{II}), adsorbed Mn^{2+} (A_{II}), and solid phase Mn (S_{II}) in the reduced layer are:

$$[(1 + K_{eq})Db + Ds]\frac{\delta^2 C_{II}}{\delta x^2} - (1 + K_{eq})\omega\frac{\delta C_{II}}{\delta x} - k_a(C_{II} - C_a) + \vartheta k_{des}(A_{II} - A_{eq}) = 0 \quad (4)$$

$$Db\frac{\delta^2 A_{II}}{\delta x^2} - \omega\frac{\delta A_{II}}{\delta x} - k_{des}(A_{II} - A_{eq}) + k_r(S_{II} - S_{eq}) = 0 \quad (5)$$

$$Db\frac{\delta^2 S_{II}}{\delta x^2} - \omega\frac{\delta S_{II}}{\delta x} - k_r(S_{II} - S_{eq}) = 0. \quad (6)$$

The six differential equations were analytically solved assuming continuity of concentrations and fluxes at the redox boundary and specific conditions at the external boundaries; i.e., the sediment-water interface and at infinite depth. At the sediment-water interface the concentration of dissolved Mn^{2+} equals that in the overlying water (C_0 is set at 0 μM), but the gradient is not necessarily zero. The fluxes of solid phase Mn and adsorbed Mn^{2+} at the sediment-water interface are $J_{Sx=0}$ and $J_{Ax=0}$, respectively. At infinite depth the concentrations of C_{II}, A_{II} and S_{II} converge to C_a, A_{eq} and S_{eq}, respectively, as their gradients and diffusive fluxes diminish. Variance-weighted sums of squares for dissolved and adsorbed Mn^{2+} as well as solid phase Mn were minimized simultaneously, while five parameters (k_{des}, k_r, k_a, $J_{Sx=0}$ and $J_{Ax=0}$) were varied to fit the model to the data using the Excel solver routine.

b. Parameter values

The values of fixed parameters are given in Table 3. The equilibrium concentration of dissolved Mn^{2+} with respect to kinetic adsorption (C_{eq}) is very small and was therefore set at zero. As no literature data on the oxidation rate of adsorbed Mn^{2+} in marine sediments are available, we tuned k_{oxa} values to obtain one suitable value for all stations. The adsorbed Mn gradient close to the redox-boundary cannot be reproduced when k_{oxa} is set lower than 0.001 d^{-1}. On the other hand, when k_{oxa} is increased substantially, the model can not fit the surface maximum unless the flux of adsorbed Mn is unrealistically high which after oxidation would result in an enhanced surface enrichment of solid phase Mn, which is not realistic either. Thus k_{oxa} was set at 0.001 d^{-1} and this value was used at all stations, except for the station at 396 m on the Nazaré Canyon transect, where the Mn profiles could only be fit with a slightly higher k_{oxa} (0.003 d^{-1}). The bioturbation coefficients are derived from ^{210}Pb profiles (Van Weering and De Stigter, 1999) and modeled according to Soetaert

Table 3. Fixed parameters used in model calculations.

Water depth (m)	(1) k_{oxc} (d^{-1})	(2) k_{oxa} (d^{-1})	(3) k_{ads} (d^{-1})	(4) Db ($m^2\ d^{-1}$)	(5) Ds ($m^2\ d^{-1}$)	(6) ω ($m\ d^{-1}$)	(7) L (m)	(8) C_a (μM)	(9) A_{eq} (μmol g^{-1})	(10) S_{eq} (μmol g^{-1})
I La Coruña Transect										
175	1	0.001	0.001	1.95E-7	1.91E-5	9.86E-8	2.5E-3	2.00	0.01	0.38
2109	1	—	—	3.04E-8	2.40E-5	1.48E-7	5.5E-2	3.00	—	1.50
II Vigo Transect										
213	1	0.001	0.001	2.30E-7	2.16E-5	1.37E-7	6.3E-3	0.50	0.01	0.70
223	1	0.001	0.001	2.30E-7	2.04E-5	1.37E-7	1.5E-2	0.10	0.02	0.36
2164	1	0.001	0.001	1.37E-9	2.21E-5	1.67E-7	9.0E-2	3.00	0.14	2.00
2213	1	0.001	0.001	3.29E-9	2.15E-5	1.67E-7	9.0E-2	3.00	0.06	1.00
3371	1	0.001	0.001	1.37E-9	2.00E-5	1.48E-7	1.0E-1	3.00	0.06	2.00
III Main Transect										
104	1	0.001	0.001	4.93E-6	3.50E-5	1.37E-7	3.8E-3	3.35	0.03	1.53
113	1	0.001	0.001	5.48E-7	2.91E-5	1.37E-7	7.5E-3	2.50	0.05	1.75
123	1	—	—	5.48E-7	2.36E-5	1.37E-7	1.5E-2	0.20	—	1.00
932	1	—	—	3.32E-8	2.40E-5	2.74E-7	2.3E-2	3.00	—	1.17
1387	1	0.001	0.001	1.07E-8	2.46E-5	1.37E-6	3.0E-2	4.00	0.17	1.50
2060	1	0.001	0.001	2.19E-9	2.33E-5	2.55E-7	8.0E-2	6.00	0.05	1.00
2073	1	0.001	0.001	2.47E-9	2.33E-5	2.55E-7	9.0E-2	6.00	0.11	2.00
IV Nazaré Canyon Transect										
137	1	0.001	0.001	1.37E-7	2.62E-5	1.37E-6	1.0E-2	1.00	0.02	1.30
396	1	0.003	0.001	1.84E-7	2.43E-5	2.74E-7	2.0E-2	1.00	0.04	1.30
344	1	—	—	1.04E-7	3.38E-5	2.74E-6	7.5E-3	1.00	—	2.80
890	1	0.001	0.001	1.10E-7	2.41E-5	2.74E-6	1.5E-2	4.00	0.15	2.20
3097	1	0.001	0.001	2.74E-7	2.32E-5	2.74E-6	1.3E-2	30.0	0.40	3.30

(1) K_{oxc} is set at 1 d^{-1} (Slomp *et al.,* 1996; Thamdrup *et al.,* 1994) (2) K_{oxa} is set to 0.001 d^{-1} (see text) (3) K_{ads} is set equal to K_{oxa} (4) Db is usually obtained from ^{210}Pb modeling (see text). (5) Ds at 35 PSU and appropriate temperature (Boudreau, 1997) corrected for porosity (Ullman and Aller, 1982) (6) Omega is the sedimentation rate (see text). (7) Oxygen penetration depth or nitrate inflection point. (8) C_a set equal or slightly lower than the deepest Mn^{2+} concentration observed. (9) A_{eq} is set equal or slightly lower than the deepest adsorbed Mn^{2+} concentration observed. (10) S_{eq} is set to the deepest solid Mn concentration measured.

et al. (1996) (Table 3 and 4). At the stations at 344 and 890 m in the canyon, ^{234}Th derived values were used (Schmidt *et al.,* 2001b). Sedimentation rates are derived from ^{14}C AMS calibrated biostratigraphy (Van Weering and De Stigter, 1999; Table 3). There are no data on sedimentation rates for stations at 104 m and 1387 m on the main transect and the shelf stations on the Nazaré Canyon transect. The values in Table 3 are optimized to fit the model to the data within a reasonable range (0.001–0.05 cm yr^{-1}). The assumed value for the sedimentation rate at the station at 104 m on the main transect has no influence on the model fit, because transport is fully dominated by mixing (Peclet number, $Pe = 10^{-4}$). The sedimentation rate for stations at 344, 890 and 3097 m in the canyon was set on 0.1 cm yr^{-1}, but using a sedimentation rate of 0.01 cm yr^{-1} did not effect any of the

Table 4. Bioturbation coefficients.

Station depth (m)	Lower limit Db ($cm^2\ yr^{-1}$)	Upper limit Db ($cm^2\ yr^{-1}$)	Used value Db ($cm^2\ yr^{-1}$)	How derived
Vigo transect				
223	—	3.84	0.84	Empirical relationship #
Main Transect				
113	0.23	3.1*	2	Empirical relationship #
123	—	5.8	2	Empirical relationship #
Nazaré Canyon Transect				
137	—	2.8	0.5	Optimized by model fitting
396	0.07	1.24**	0.67	Optimized by model fitting
3097	—	2.9**	1	Optimized by model fitting

Empirical relationship between mixing coefficient and water depth in the OMEX I area at the Goban Spur farther to the north on the European continental margin (Soetaert *et al.,* 1996).

**Db* values derived from ^{234}Th data (Schmidt *et al.,* 2001a).

***Db* values derived from ^{234}Th data (Schmidt *et al.,* 2001b).

When the sedimentation rate used for the calculation of the *Db* is a lower estimate, then the resulting ^{210}Pb derived *Db* is an upper estimate.

integrated Mn reaction rates more than 6%. The Mn model of Slomp *et al.* (1997) was applied to the profiles of solid phase Mn and pore water Mn^{2+} to obtain reduction and oxidation rates for the 2109 m station on the La Coruña transect and the 123 m station on the main transect, since adsorbed Mn^{2+} data were not available for these two stations. This model was also used at the station at 932 m on the main transect, where the adsorbed Mn profile was rather uniform with depth.

5. Experimental results

Profiles of the stations on the *La Coruña transect* are shown in Figure 4. At the shallow station the solid phase Mn profile has its maximum at the sediment-water interface, whereas adsorbed Mn has its maximum slightly deeper; i.e., in-between those of solid phase Mn and pore water Mn^{2+}. The concentrations of both solid phase and pore water Mn are highest at the 2109-m station. At the deeper 4908 and 4941-m stations pore water Mn^{2+} concentrations are low. The increase of solid phase Mn with depth at 4908 m suggest a solid phase Mn maximum deeper than 200 mm.

On the *Vigo transect,* the pairs of stations sampled in August and May at approximately 200, 2200 and 2900 m water depth were almost at the same location (Table 1). The corresponding profiles are not identical, but they do show the same pattern (Fig. 5). At the two shallowest stations concentrations of solid phase Mn are low and the maximum in adsorbed Mn is close to the sediment-water interface. Concentrations of solid phase Mn are one order of magnitude higher at the deeper stations (2164, 2213 and 3371 m).

On the *Main transect* three shallow stations were sampled of which the stations 104 and

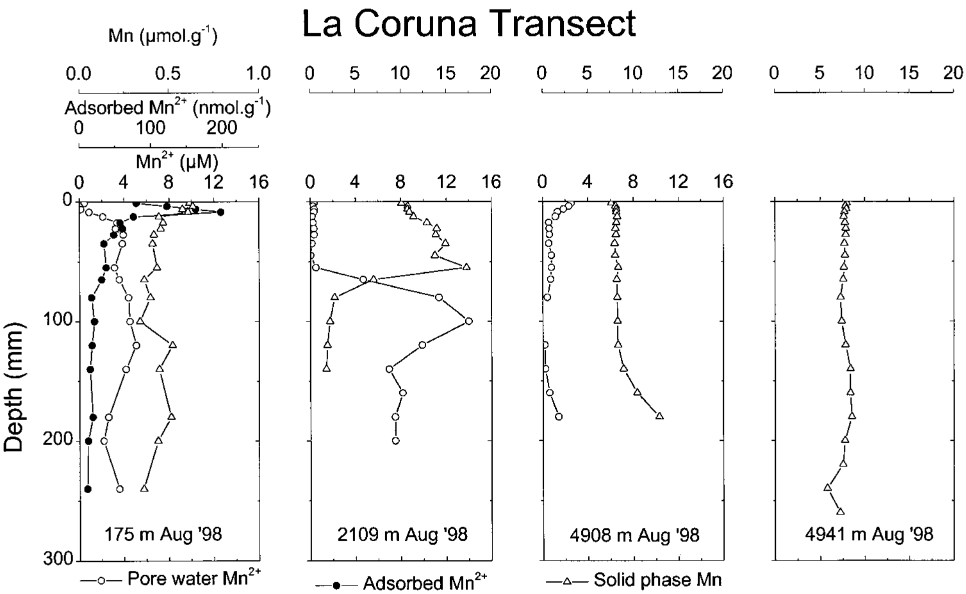

Figure 4. Vertical profiles of pore water Mn^{2+}, adsorbed Mn^{2+} and solid Mn of the stations on the La Coruña transect. Note the different scales for solid Mn at the shallow and the deeper stations.

113 m are located in a mud patch and show slightly higher concentrations than the other shallow station at 123 m (Fig. 6). The highest concentration of adsorbed Mn^{2+} (note scale) and pore water Mn^{2+} is observed at the 1387-m station.

On the *Nazaré Canyon transect* four stations were sampled in the canyon and two stations (137 and 396 m) outside (Fig. 7). The latter two show much lower concentrations of all Mn species than the stations located in the canyon. Remarkably high concentrations of adsorbed Mn^{2+} are found in the canyon stations at 346, 890 and 3097 m, comparable to the 1387 m station on the main transect. Pore water Mn^{2+} concentrations at the 3097-m station reach almost 50 μM, which is much higher than in any of the other profiles. Except for the deepest station, the down-core sequence of maxima is the same as at all stations; i.e., the adsorbed Mn^{2+} maximum is in-between those of solid phase Mn and pore water Mn^{2+}. The deepest canyon station is different from the others, because it consists of alternating layers of Mn poor sand and Mn rich clay with very little adsorbed Mn^{2+}, but high pore water Mn^{2+} concentrations.

At the noncanyon transects oxygen fluxes ranged from 2.9 to 10.9 mmol $O_2\ m^{-2}\ d^{-1}$ at depths <400 m, decreasing to ca 0.6 mmol $O_2\ m^{-2}\ d^{-1}$ at depths exceeding 1000 m (Fig. 8). Applying an oxygen to carbon stoichiometry of 138:106 for aerobic mineralization, these oxygen fluxes are equivalent to organic carbon mineralization rates of 9.8 to 37 g C $m^{-2}\ y^{-1}$ at depths <400 m and 2 g C $m^{-2}\ y^{-1}$ at greater water depths (>1000 m). At the canyon transect, the oxygen fluxes are equivalent to organic carbon mineralization rates of 13.5, 6.1, and 3.7 g C $m^{-2}\ y^{-1}$, respectively. The carbon mineralization rates for

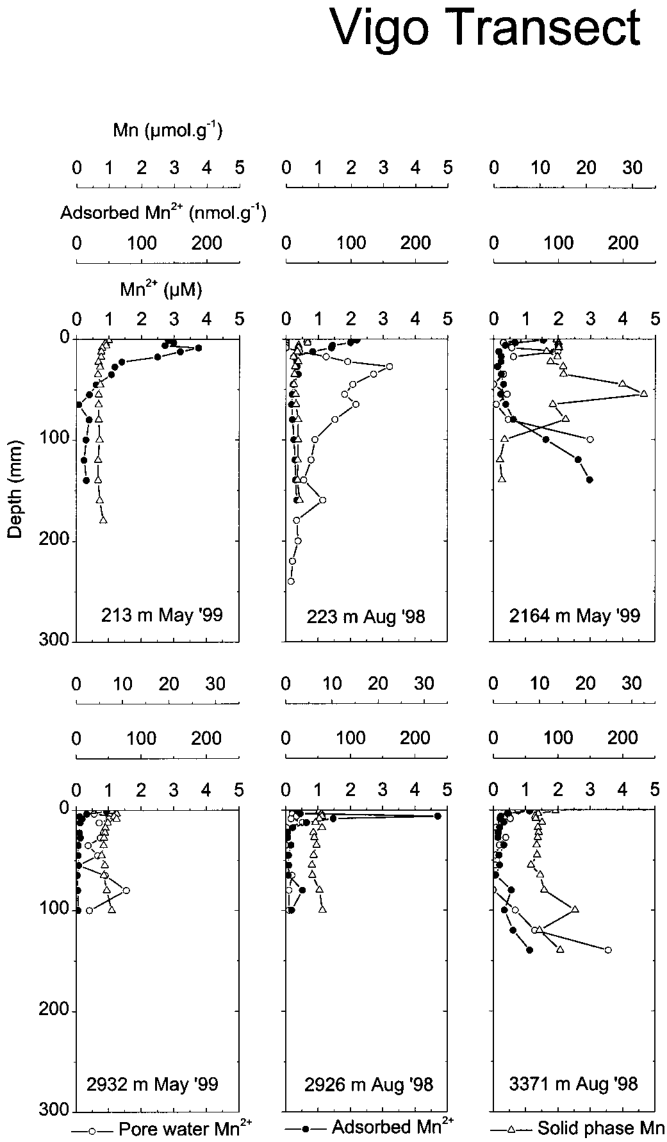

Figure 5. Vertical profiles of pore water Mn^{2+}, adsorbed Mn^{2+} and solid Mn of the stations on the Vigo transect. Note the different scales for solid Mn at the shallow and the deeper stations.

344 m water depth are well within the range of the other shelf stations, whereas the rates at 3097 and 4280 m water depth exceed the estimates for corresponding water depths along the other transects by a factor of 3 and 2, respectively. More details on carbon cycling will be discussed by Epping *et al.* (2001).

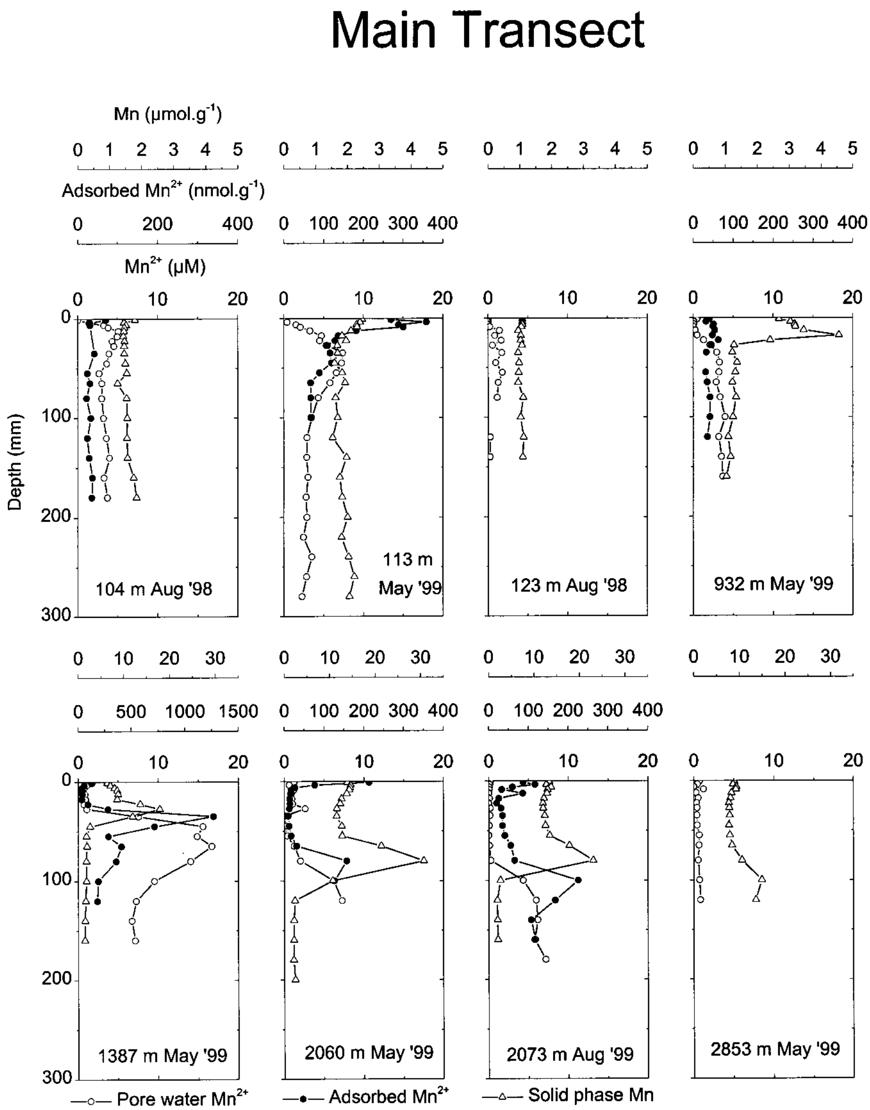

Figure 6. Vertical profiles of pore water Mn^{2+}, adsorbed Mn^{2+} and solid Mn of the stations on the Main transect. Note the different scales for solid Mn at the shallow and the deeper stations.

6. Model results

The model was applied to stations where data of dissolved Mn^{2+}, adsorbed Mn^{2+} and solid phase Mn were available. The profiles of most stations deeper than 3000 m were not modeled because the major redox transitions apparently occurred deeper than our sampling interval. The profiles of the deepest canyon station could not be modeled due to the alternating layers of Mn-rich clay and Mn-poor sand. The values of the fitted parameters

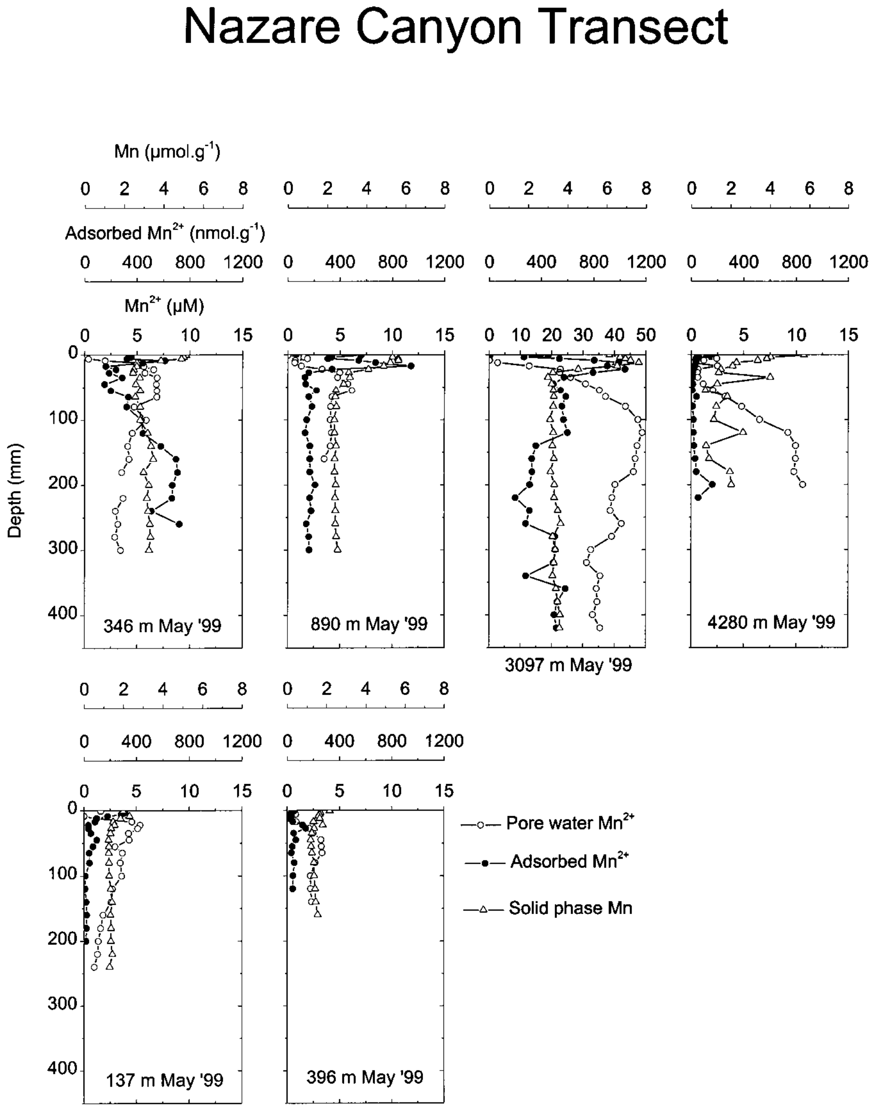

Figure 7. Vertical profiles of pore water Mn^{2+}, adsorbed Mn^{2+} and solid Mn of the stations on the Nazaré Canyon transect. Note the different scale for pore water Mn^{2+} at the 3097-m station.

are given in Table 5. The model fits the data reasonably well and the sequence of peaks is well reproduced (Fig. 9a–d). A recurring deviation of the model fit from the data is observed in the background concentration of adsorbed Mn^{2+} in the oxic layer. The model fit of the solid phase profile of the station at 2213 m on the Vigo transect (Fig. 9b) is a typical compromise of fitting both the maximum at the redox boundary and the surface enrichment. The values for the first-order rate constants vary over several orders of

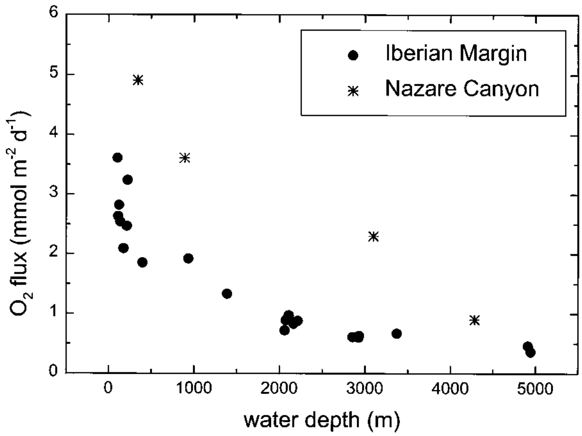

Figure 8. Benthic oxygen fluxes as a function of water depth on the margin (filled circles) and in the canyon (asterisk).

Table 5. Values for k_{des}, k_r, k_a, $J_{Sx=0}$ and $J_{Ax=0}$ obtained by fitting the model to the data.

Water depth (m)	k_{des} (d^{-1})	k_r (d^{-1})	k_a (d^{-1})	$J_{Sx=0}$ ($\mu mol \cdot m^{-2} \cdot d^{-1}$)	$J_{Ax=0}$ ($\mu mol \cdot m^{-2} \cdot d^{-1}$)
I La Coruña Transect					
175	4.33E-4	1.18E-3	1.70E-3	0.95	0.96
2109	—	1.09E-4	1.29E-3	1.05	—
II Vigo Transect					
213	2.29E-3	7.15E-3	1.02E-1	5.81	0.25
223	5.01E-3	1.62E-2	1.20E-2	0.65	0.87
2164	5.44E-2	5.25E-4	5.10E-1	1.51	0.14
2213	2.81E-2	8.47E-5	9.47E-2	0.71	0.22
3371	1.63E-2	1.03E-6	2.68E-3	1.05	0.12
III Main Transect					
104	6.42E-1	3.85E-2	1.19E-1	0.92	15.3
113	2.93E-3	1.42E-3	2.75E-2	5.15	4.32
123	—	4.37E-3	1.83E-2	0.18	—
932	—	3.82E-4	1.98E-2	0.31	—
1387	1.55E-3	2.46E-4	4.67E-3	5.05	0.55
2060	4.23E-3	3.04E-5	5.10E-2	1.43	0.45
2073	1.97E-2	1.68E-3	1.55	1.39	0.37
IV Nazaré Canyon Transect					
137	4.05E-3	6.24E-4	8.56E-3	0.80	4.65
396	2.30E-3	1.10E-2	3.77E-3	0.59	0.59
344	—	4.22E-3	3.55E-4	4.27	—
890	3.95E-3	2.23E-3	2.60E-1	7.52	2.29
3097	2.92E-3	1.18E-3	8.23E-5	11.1	0.20

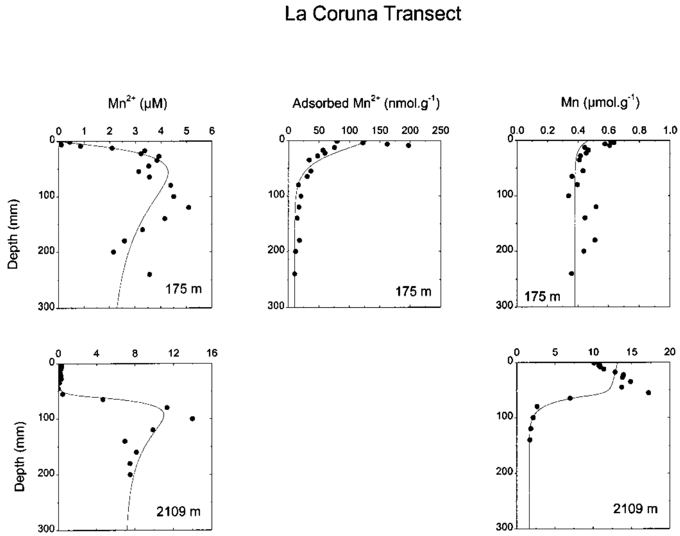

Figure 9. Model fits (lines) to profiles of pore water Mn^{2+}, adsorbed Mn^{2+} and solid Mn (filled circles) of the stations on the (a) La Coruña, (b) Vigo, (c) Main and (d) Nazaré Canyon transect.

magnitude (Table 5) and are comparable to those obtained in a similar way for North Sea sediments (Slomp *et al.,* 1997) and for east equatorial Pacific sediments (Burdige and Gieskes, 1983). According to Slomp *et al.* (1997), large variation in the first-order rate constants is due to the lumping of a number of processes in one rate constant, which depend on several factors, e.g., the reactivity of the Mn oxide and the type of reductant involved. Burdige and Gieskes (1983) mention differences in surface area and/or mineralogy of the solids, temperature differences, bacterial versus inorganic catalysis and organic matter reactivity to cause differences in rate constants. Sensitivity analyses for the rate constants presented here were conducted by fixing one constant at several values around its optimum and re-fitting the profiles. Fits were least sensitive to the reduction and precipitation rate constants probably because precipitation is not constrained by a (Ca,Mn)-CO_3 profile and desorption is relatively fast. Model fits are more sensitive to the desorption rate constant.

In contrast to the wide range of reaction rate constants is the confined range of the integrated rates of reduction, desorption and oxidation, which were calculated with the model (Table 6), indicating that the overall rates of Mn cycling are not controlled solely by their first order rate constants, but that their combined actions, pool sizes and transport rates are important as well. The Mn reduction rates range between 1 and 35 μmoles m^{-2} d^{-1}, whereas desorption and oxidation rates range from 1 to 30 μmoles m^{-2} d^{-1}. The depth integrated rates of desorption are generally slightly lower than those of reduction. Therefore, only a small amount of adsorbed Mn^{2+} can be found in the deeper part of the profiles. Desorption is more intense than reduction when the redox boundary is very close to the sediment-water interface and the deposition flux of adsorbed Mn^{2+} releases Mn^{2+}

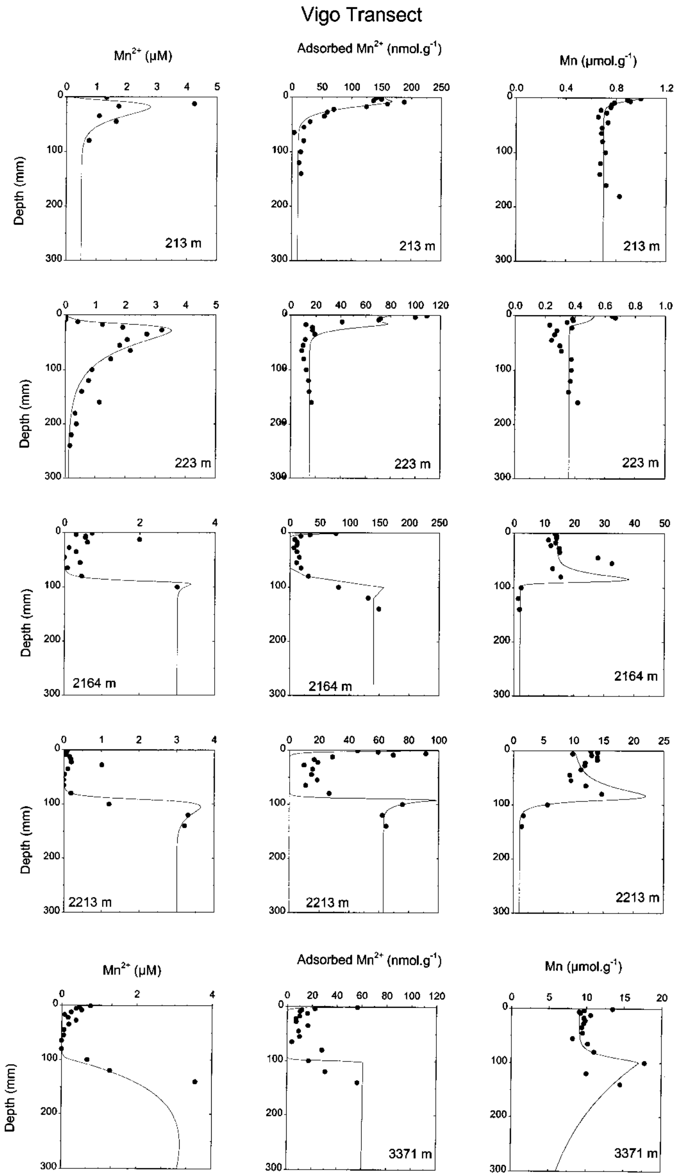

Figure 9. (continued)

into the pore water directly. The Mn oxidation rates are lower than the reduction rates except at the station at 137 m on the Nazaré Canyon transect, where the oxidation is slightly faster due to direct oxidation of the deposition flux of adsorbed Mn^{2+}. The rates of reduction, desorption and oxidation at the non-canyon stations show a maximum around

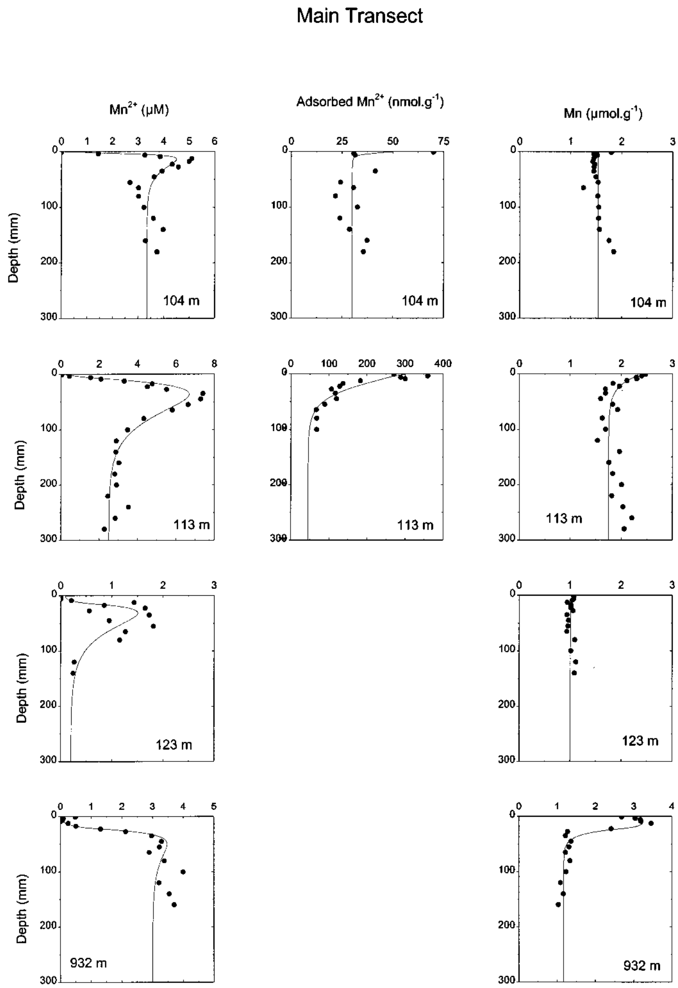

Figure 9. (continued)

1400 m water depth (Fig. 10). The rates of reduction, desorption and oxidation are relatively high at the 3097-m canyon station compared to stations on the margin at similar water depth. Although the profiles from the deepest canyon station at 4280 m could not be modeled, the reduction and oxidation rate are likely to be lower than at the 3097-m station. The slope of the pore water profile is steeper at the 3097-m station than at the 4280-m station, moreover the pore water concentrations are highest at the 3097-m station. The maximum reduction, desorption and oxidation rates on the Nazaré Canyon transect occur at greater water depth than at the other three transects.

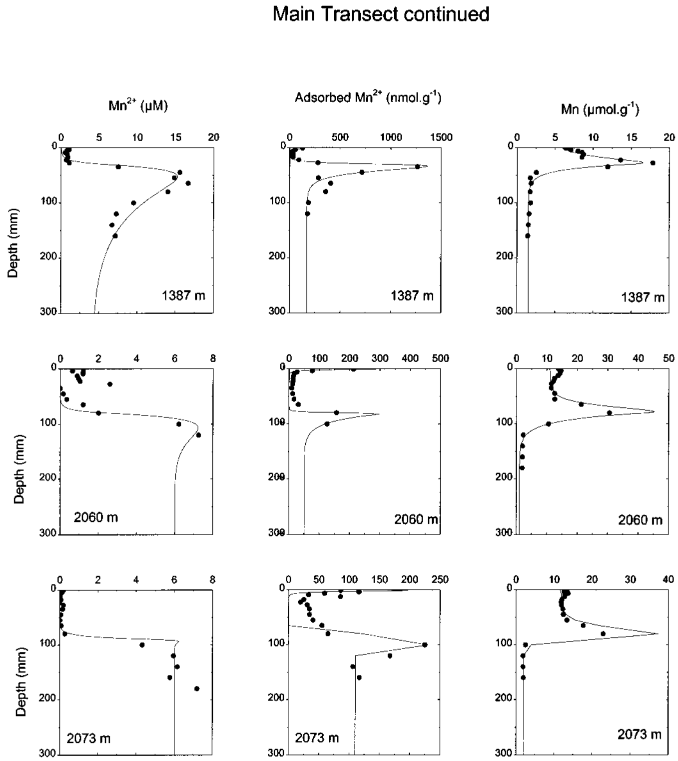

Figure 9. (continued)

7. Discussion

a. Iberian margin versus other margins

Manganese is most important as intermediate oxidant in areas with (1) well-oxygenated overlying water, which minimizes the loss of Mn^{2+} from the sediment, (2) high bioturbation, which enhances the Mn redox cycle by mixing oxidized and reduced sediment layers, and (3) moderate organic carbon fluxes (Aller, 1994). When relatively large amounts of hydrothermal manganese are supplied to the sea floor in addition to moderate carbon fluxes, Mn cycles driven by bioturbation can account for up to 100% of the organic matter mineralization as described for the Panama Basin (Aller, 1990).

At the eastern Canadian continental margin bottom waters are well oxygenated and model calculations showed that at a water depth of 230 m 2% of the carbon oxidation could be contributed to Mn reduction, at 525 m 16%, whereas at 780 m no Mn^{2+} was detected in the upper 10 cm (Boudreau *et al.,* 1998). In general, however, Mn reduction is a minor mineralization pathway at continental margins (Archer and Devol, 1992; Reimers *et al.,* 1992; Thamdrup and Canfield, 1996; Lohse *et al.,* 1998). Assuming a stoichiometry of organic C oxidation: Mn reduction of 1:2, the maximum contribution of Mn reduction to

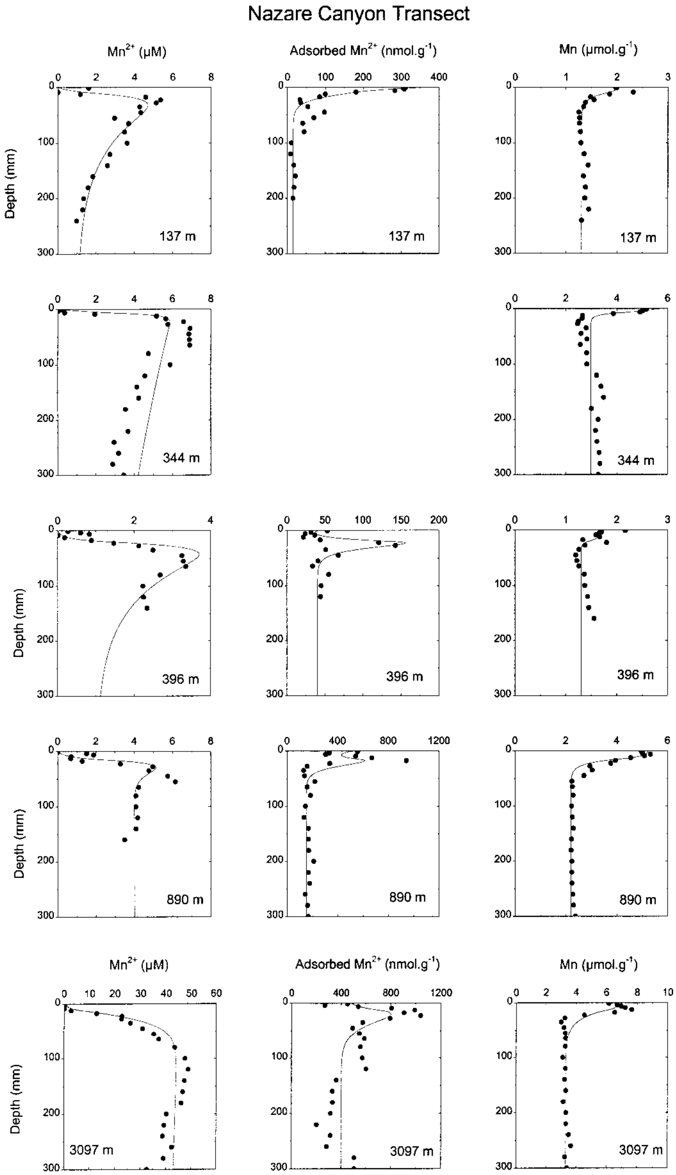

Figure 9. (continued)

the organic matter oxidation is <2% at the Iberian margin. The reduction rates found in this study are comparable with those of an earlier study in the framework of the OMEX-I programme at the Goban Spur on the N.W. European continental margin (Lohse *et al.*, 1998).

Table 6. Calculated integrated rates of reduction, desorption, oxidation and precipitation of Mn and the Mn^{2+} flux out of the sediment from values obtained by fitting the model to the data.

Water depth (m)	Red. rate ($\mu mol \cdot m^{-2} \cdot d^{-1}$)	Des. rate ($\mu mol \cdot m^{-2} \cdot d^{-1}$)	Ox. rate ($\mu mol \cdot m^{-2} \cdot d^{-1}$)	Precip. rate ($\mu mol \cdot m^{-2} \cdot d^{-1}$)	Mn^{2+} flux out ($\mu mol \cdot m^{-2} \cdot d^{-1}$)
La Coruña Transect					
175	1.60	2.11	0.72	0.28	1.56
2109	11.5	—	10.6	0.76	0.37
4908	#	#	#	#	#
4941	#	#	#	#	#
Vigo Transect					
213	8.72	7.70	3.03	4.25	1.68
223	5.43	4.80	4.84	1.19	0.26
2164	10.8	10.6	9.49	1.41	0
2213	7.24	7.12	6.65	1.13	0
3371	2.05	2.00	1.26	0.93	0
Main Transect					
104	3.88	19.0	3.17	2.73	13.3
113	11.5	14.0	6.52	5.68	3.57
123	2.46	—	1.81	0.75	0.10
932	4.73	—	4.70	0.27	0.24
1387	25.3	23.3	21.8	3.74	0.09
2060	11.4	11.2	10.1	1.69	0
2073	21.5	20.7	20.4	1.44	0
2853	#	#	#	#	#
Nazaré Canyon Transect					
137	5.99	8.07	6.98	1.94	1.70
396	7.91	4.62	7.71	0.64	0.14
344	17.5	—	8.69	0.15	9.64
890	16.9	15.3	12.6	5.47	0.92
3097	34.9	29.4	29.5	0.50	4.27

Profiles were not modeled because the major redox transitions apparently were positioned deeper than our sampling interval. The rates are assumed to be close to zero.

b. *Canyon versus other transects*

Some stations were sampled both in August 1998 and May 1999, but seasonal fluctuations in the Mn redox chemistry, if present, were not observed. No trend was observed going from north to south on the Iberian margin. However, a large difference in Mn reactivity was found between the stations on the margin and those in the canyon. The highest integrated Mn reaction rates were estimated for the station at 3097 m in the canyon. Reaction rates are higher at the canyon stations compared to those at similar water depth on the margin, indicating a more rapid Mn redox cycling in the canyon. Mass accumulation rates in the canyon are higher than on the shelf with a maximum at the 3097-m station (Van Weering *et al.,* 2001). Along with this higher sedimentation rate is the estimated flux of Mn

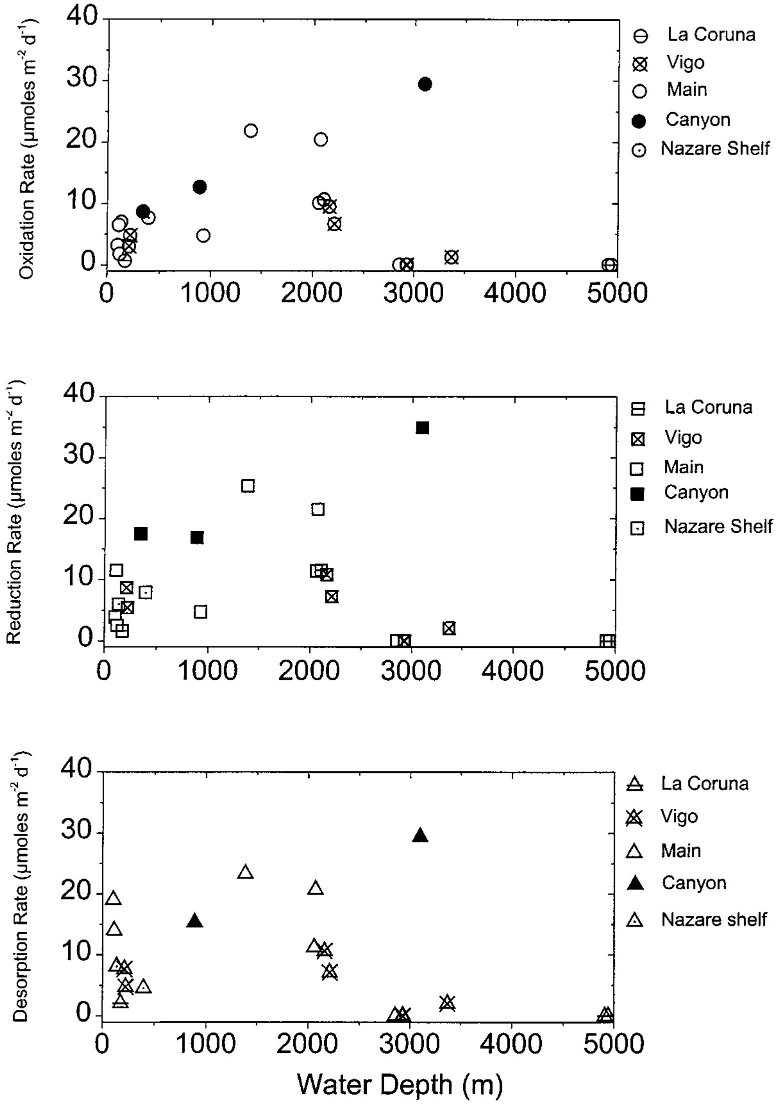

Figure 10. Mn^{2+} oxidation rate, Mn reduction rate and Mn^{2+} desorption rate as a function of water depth.

oxides ($J_{Sx=0}$, Table 5) increases with increasing water depth at the canyon transect from 344 to 3097 m, whereas a trend with water depth is less clear at the other transects. Estimated Mn oxide deposition fluxes at the 890 and 3097-m stations in the canyon exceed the Mn oxide fluxes at all other stations. Thus, Mn cycling in the canyon is enhanced at higher input fluxes of Mn oxides.

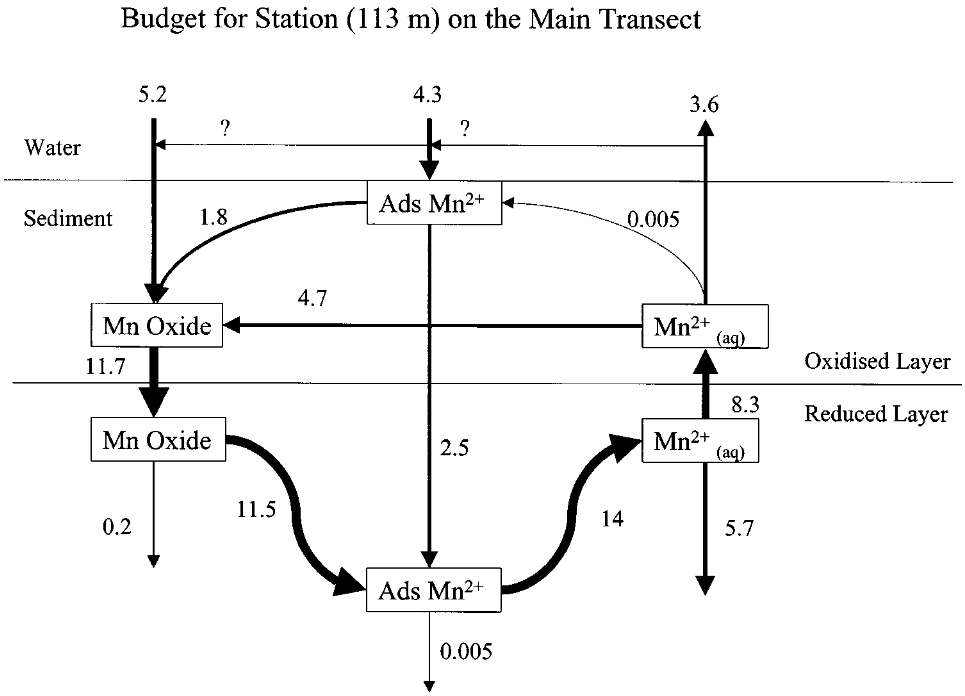

Figure 11. Fluxes of Mn in µmoles m^{-2} d^{-1} as calculated with the model for the 113-m station on the main transect.

c. Rate limiting factors

Budgets were constructed from the model results for the 113-m station (Fig. 11) and the 1387-m station on the main transect (Fig. 12), and for the 3097-m station in the canyon (Fig. 13). The major pathway for redox cycling starts when Mn oxide is mixed and/or advected into the reduced layer. There, adsorbed Mn^{2+} is produced by Mn reduction and subsequently is desorbed and released into the pore water. The Mn^{2+} diffuses upward into the oxidized layer and is oxidized. When the oxidized layer is relatively thin some Mn^{2+} can escape from the sediment as is shown for the 113-m station (Fig. 11) and the canyon station (Fig. 13). Mn^{2+} in the water column may adsorb or oxidize onto sinking particles, indicated by the arrow with question mark in the budgets (Figs. 11–13) and subsequently re-enter the sediment. The species with the longest turnover time, i.e., the rate limiting pools in Mn cycling, are listed in Table 7. In general, at shallow stations (<225 m) and at the 3097-m station in the canyon, the slowest turnover occurs in the oxidation step of adsorbed Mn^{2+}. At the other stations the transport of Mn oxide from the oxidized to the reduced layer is the rate-limiting step for Mn cycling. Thus, the rate limiting factors for Mn redox cycling at the Iberian margin are slow oxidation kinetics and slow mixing.

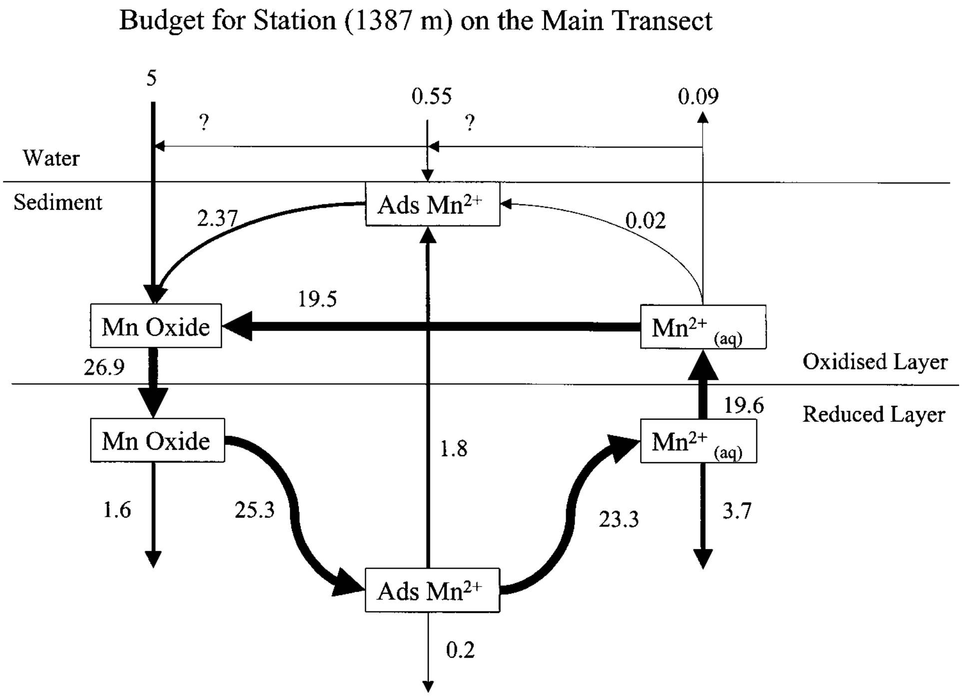

Figure 12. Fluxes of Mn in μmoles m^{-2} d^{-1} as calculated with the model for the 1387-m station on the main transect.

d. What controls the Mn redox chemistry?

Klinkhammer (1980) and Burdige and Gieskes (1983) subdivided the sediment column into four distinct zones based on the Mn redox chemistry. In our model, the sediment column was divided in an oxidized and a reduced layer with depth L as the Mn redox boundary. However, these layers can be subdivided into two zones each, i.e., the oxidized layer consisting of a fully oxidized zone and an oxidizing zone, and the reduced layer consisting of a reducing zone and an equilibrium zone. We extended the sediment zonation of Klinkhammer (1980) and Burdige and Gieskes (1983) by including adsorbed Mn^{2+} as indicated in Figure 14. Depending on the depth of the Mn redox boundary in the sediment and the core length, one to four of these zones could be identified within the sampled interval. Based upon their Mn zonation and the concentrations of the three Mn species, all noncanyon stations can be divided into three groups, each category corresponding to a limited water depth range. The first group of shallow stations (100–400 m) is characterized by low concentrations of both solid phase Mn and pore water Mn^{2+}. The solid phase Mn profile has its maximum at the sediment-water interface, whereas the adsorbed Mn has its maximum either at the sediment-water interface or just below. Thus, at the shallow stations only a reducing and an equilibrium zone can be identified, the oxidizing zone being too

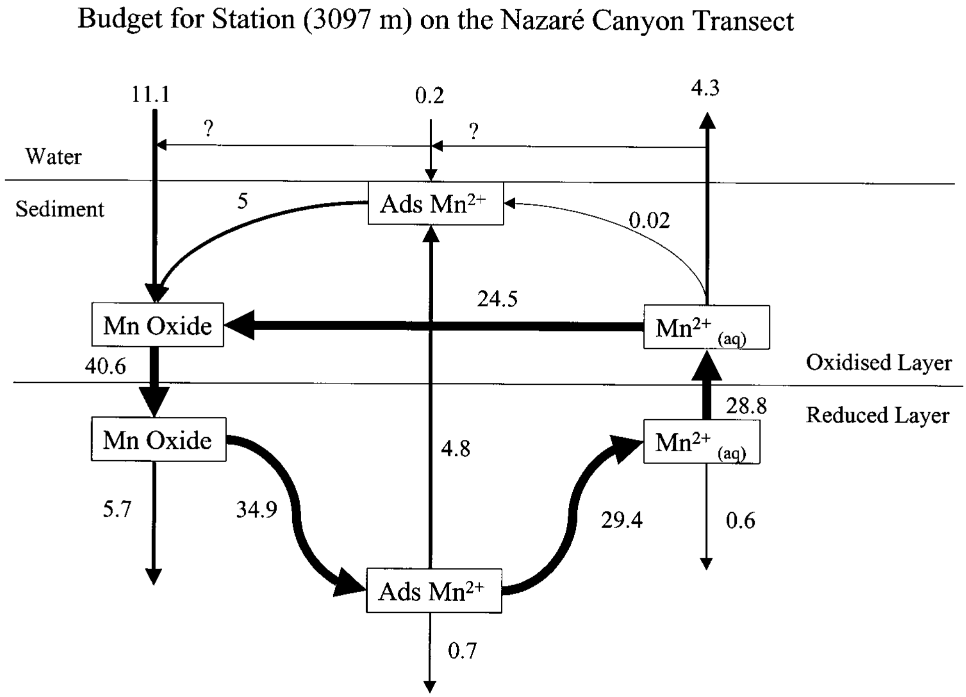

Figure 13. Fluxes of Mn in μmoles m^{-2} d^{-1} as calculated with the model for the 3097-m station on the Nazaré Canyon transect.

strongly compressed to be sampled adequately. In the second group of stations at intermediate water depth (900–2300 m) all four zones, i.e., an oxidized, an oxidizing, a reducing and an equilibrium zone can be distinguished. Their solid phase Mn concentrations are one order of magnitude higher than at the shallow stations. Pore water concentrations are similar to or higher than those of the shallow stations, whereas the adsorbed Mn^{2+} concentrations are similar, except at the station at 1387 m (main transect) which has much higher values. In the third group of stations at greater depth (>2300 m), one to two zones were observed, i.e., an oxidized and oxidizing zone. Pore water Mn^{2+} concentrations are negligible and adsorbed Mn^{2+} is slightly enriched at the sediment surface only. The solid phase Mn concentrations are constant with depth, characteristic of a well oxidized zone, or increase slightly with depth indicating the onset of an oxidizing zone deeper down.

In general, sediment mixing is higher at stations with a high carbon flux (Boudreau, 1998), which would increase Mn reaction rates. The stations with high carbon fluxes (Fig. 8) are the shallow stations and their rate-limiting factor in the Mn cycle is the oxidation of Mn^{2+} (see previous section). The oxygen penetration depths (L, Table 3) are shallow and the oxidation kinetics are too slow to prevent a Mn^{2+} efflux across the thin

Table 7. Slowest cycling fraction estimated using the model results and the rate limiting process.

Water depth (m)	Slowest fraction*	In layer**	Rate limiting process
La Coruña Transect			
175	Ads	red	desorption
2109	Ox	—	mixing
4908	—	—	
4941	—	—	
Vigo Transect			
213	Ads	ox	oxidation
223	Ads	ox	oxidation
2164	Ox	ox	mixing
2213	Ox	ox	mixing
3371	Ox	red	
Main Transect			
104	Ads	ox	oxidation
113	Ads	ox	oxidation
123	Ox	—	mixing
932	Ox	—	mixing
1387	Ox	ox	mixing
2060	Ox	ox	mixing
2073	Ox	ox	mixing
2853	—	—	
Nazaré Canyon Transect			
137	Ads	ox	oxidation
396	Ox	ox	mixing
344	Ox	—	mixing
890	Ox	ox	mixing
3097	Ads	ox	oxidation

*Ads is the adsorbed Mn phase and Ox is the solid phase Mn. The slowest fraction is the fraction with the largest turnover time calculated from the standing stock (μmol m^{-2}) divided by the production rate (μmol m^{-2} d^{-1}).

**Ox is the oxidized layer and red is the reduced layer.

oxic layer (Table 6), resulting in a lowered availability of Mn oxide relative to organic carbon. Mn fluxes at shallow stations at the Iberian margin are limited by Mn oxide regeneration. At stations with low mineralization rates the oxygen penetration depth is in the order of several cm and deeper. At the depth level where oxygen is depleted in the sediment, the organic matter reaching the Mn reduction zone is aged and probably refractory. Therefore Mn reaction rates at stations at water depths >2300 m at the Iberian margin are limited by the availability of reductants, be they organic or inorganic. Thus, Mn fluxes are highest at stations with moderate organic carbon fluxes, where carbon flux and its degradability control the Mn redox chemistry.

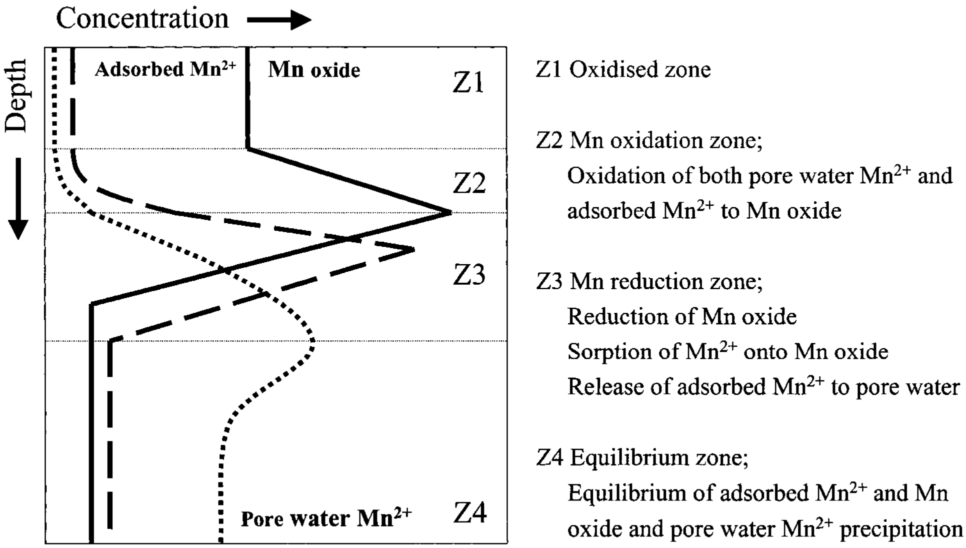

Figure 14. Manganese zonation scheme for pore water Mn^{2+}, adsorbed Mn^{2+} and Mn oxide profiles. Dominant processes in each layer are described.

e. The role of Mn^{2+} sorption in Mn redox cycling

Adsorbed Mn^{2+} can be an important reaction intermediate in the redox transformations of Mn especially in the reduced layer. Our results show that adsorbed Mn^{2+} has its maximum in-between those of solid phase Mn and pore water Mn^{2+}. Hence, we propose that upon Mn reduction the produced Mn^{2+} is adsorbed at nearby Mn oxide surfaces. Available adsorption-sites on the Mn-oxide are diminished and/or saturated upon continued Mn reduction and Mn^{2+} is released into the pore water deeper in the sediment. When Mn^{2+} diffuses upwards it is either oxidized directly or adsorbed onto Mn oxide surfaces in the oxic layer. Junta and Hochella (1994) showed that oxidation of $Mn^{2+}_{(aq)}$ starts through adsorption along edges (nm scale) on the mineral surfaces, suggesting that the geometric character of the mineral surface is more important than the immediate coordination environment. However, structural data on the Mn oxide birnessite identified a specific sorption site that consisted of three oxygen atoms carrying a double charge (-2) located around a vacancy in the octahedral layer (Drits *et al.,* 1997). Appelo and Postma (1999) formulated a surface complexation model for birnessite based on this doubly charged sorption site, which described experimental data better than monodentate or bidentate complexation models. Friedl *et al.* (1997) identified H^+-birnessite as authigenic Mn oxide in a eutrophic lake and their EXAFS spectra showed large amounts of adsorbed cations at the vacancies of its octahedral layers. Thus, Mn oxides in marine sediments may be important carriers of Mn^{2+} as well, either through sorption at specific vacancies in the crystal lattice or along edges and irregularities on the mineral surface.

The enrichment of adsorbed Mn^{2+} at the sediment-water interface suggests that the input of adsorbed Mn^{2+} is associated with recently arrived organic matter. However, adsorbed Mn^{2+} formed in the sediment is likely to be associated with Mn oxides. Small amounts of adsorbed Mn^{2+} associated with Mn oxides persist under oxygenated conditions. This can be explained by the assumption that two types of surface species exist, i.e., mono- and bidentate complexes. Davis and Morgan (1989) argue that the Mn^{2+}-bidentate complex is more readily oxidized than the monodentate complex.

Allocation of Mn^{2+} from the pore waters to the solid phase, would in principle result in a reduced pore water gradient of Mn^{2+} at the sediment-water interface and consequently in a lowered efflux of Mn^{2+}. However, this sorptive immobilization of dissolved Mn^{2+} moving upwards is possible only when adsorption is sufficiently rapid. In our model, the direct oxidation rate constant k_{oxc} is 1000 times k_{ads} implying that oxidation has a far larger impact on the Mn^{2+} gradient in the oxidized layer than adsorption. Kinetic Mn^{2+} sorption lowers, however, the pore water gradient in the Mn reduction zone (Z3 in Fig. 14). At shallow stations, the fully oxidized zone is absent (Z1) and the Mn oxidation zone (Z2) is so strongly compressed that the pore water gradient in the Mn reduction zone (Z3) is decisive for the Mn^{2+} efflux. Thus, kinetic sorption retains the Mn^{2+} efflux at stations with a thin oxidation zone.

8. Conclusions

Adsorbed Mn^{2+} is an important reaction intermediate in the redox transformations of Mn especially in the reduced layer between Mn oxide and pore water Mn^{2+}. The implication of an intermediate adsorbed Mn^{2+} phase is a stronger retention of Mn redox cycling in the sediment column at stations with a thin oxidation zone, since adsorbed Mn^{2+} restrains the Mn^{2+} efflux from the pore water to the water column. Adsorbed Mn^{2+} seems to be associated with organic matter upon arrival at the sea floor, whereas the adsorbed Mn^{2+} formed in the sediment is likely to be adsorbed onto Mn oxides. The major pathway for Mn redox cycling starts when Mn oxide is mixed and/or buried below the Mn redox boundary. There, adsorbed Mn^{2+} is formed during Mn oxide reduction. As available sorption sites are diminished and/or saturated, adsorbed Mn^{2+} is desorbed upon continued Mn reduction and released into the pore water. Pore water Mn^{2+} diffuses upward and is oxidized by molecular oxygen to form Mn oxide or is co-precipitated with carbonates.

The non-canyon stations could be divided into three groups based upon their pore water Mn^{2+}, adsorbed Mn^{2+} and solid phase Mn characteristics and this division coincided with water depth, i.e., shallow stations (100–400 m), stations at intermediate water depth (900–2300 m) and stations at greater water depth (>2300 m). As the flux of carbon and its degradability decreases with increasing water depth (Epping *et al.,* 2001), this suggests that the carbon flux is the main factor controlling Mn redox cycling. By application of a simple reaction-diffusion model, we have shown that the profiles of solid, adsorbed and pore water Mn are consistent. Mn reaction rates are highest at moderate carbon fluxes and are enhanced by a higher deposition flux of Mn oxide in the canyon. The two important rate-limiting factors for the Mn cycling deduced from turnover times of Mn species are (1) slow oxidation kinetics at the shallow stations (<225 m) and the 3097-m canyon station and (2) slow mixing of Mn oxides at the other stations.

Acknowledgments. The authors would like to thank the captain and crew of the R.V. *Pelagia* for providing safe cruises and a pleasant working environment. Shipboard nutrient analyses were performed by Karel Bakker, Jan van Ooijen and Evaline van Weerlee (NIOZ, Department of Marine Chemistry and Geology). Grain size data were kindly provided by Wim Boer, Henko de Stigter and Tjeerd van Weering. The investigations were carried out in the framework of the Sedimentary Manganese and Iron cycLEs project (SMILE). C.v.d.Z. was supported through a grant to W.v.R. by the Research Council for Earth and Life Science (ALW) with financial aid from the Netherlands Organisation for Scientific Research (NWO) (no. 750.297.01). We thank Willem Helder for critically reading the manuscript. E.E. was supported through a grant to W.H. by the European Community EC-MAST OMEX-II project (MAS3-CT96-0056). This is publication no. 3487 of the Netherlands Institute for Sea Research.

APPENDIX

Solutions to differential equations

$$C_I = B1\mathrm{Exp}(e1x) + B2\mathrm{Exp}(e2x)$$

$$+\ C_{II} = I\mathrm{Exp}(e10x) + \iota H\mathrm{Exp}(e8x) + \upsilon G\mathrm{Exp}(e6x) + C_a$$

$$A_I = J1\mathrm{Exp}(e3x) + J2\mathrm{Exp}(e4x) - \lambda B1\mathrm{Exp}(e1x) - \mu B2\mathrm{Exp}(e2x) + \frac{k_{ads}}{\theta \cdot k_{oxa}}\left\{\frac{k_{ads} \cdot C_{eq}}{k_{ads} + k_{oxc}} - C_{eq}\right\}$$

$$A_{II} = H\mathrm{Exp}(e8x) + \rho G\mathrm{Exp}(e6x) + A_{eq}$$

$$S_I = F1\mathrm{Exp}(\omega \cdot x/Db) - J1\mathrm{Exp}(e3x) - J2\mathrm{Exp}(e4x) + \gamma B1\mathrm{Exp}(e1x) + \varepsilon B2\mathrm{Exp}(e2x) + F2$$

$$S_{II} = G\mathrm{Exp}(e6x) + S_{eq}$$

$$e1 = \frac{\omega\,(1 + K_{eq}) + \sqrt{(\omega\,(1 + K_{eq}))^2 + 4[(1 + K_{eq})Db + Ds](k_{oxc} + k_{ads})}}{2[(1 + K_{eq})Db + Ds]}$$

$$e2 = \frac{\omega\,(1 + K_{eq}) - \sqrt{(\omega\,(1 + K_{eq}))^2 + 4[(1 + K_{eq})Db + Ds](k_{oxc} + k_{ads})}}{2[(1 + K_{eq})Db + Ds]}$$

$$e3 = \frac{\omega + \sqrt{\omega^2 + 4Dbk_{oxa}}}{2Db}$$

$$e4 = \frac{\omega - \sqrt{\omega^2 + 4Dbk_{oxa}}}{2Db}$$

$$e6 = \frac{\omega - \sqrt{\omega^2 + 4Dbk_r}}{2Db}$$

$$e8 = \frac{\omega - \sqrt{\omega^2 + 4Dbk_{des}}}{2Db}$$

$$e10 = \frac{\omega - \sqrt{\omega^2 + 4Dbk_a}}{2Db}$$

$$\iota = \frac{-\theta \cdot k_{des}}{[(1 + K_{eq})Db + Ds](e8)^2 - (1 + K_{eq})\omega \cdot e8 - k_a}$$

$$\upsilon = \frac{-\theta \cdot k_{des}\rho}{[(1 + K_{eq})Db + Ds](e6)^2 - (1 + K_{eq})\omega \cdot e6 - k_a}$$

$$\lambda = \frac{k_{ads}}{\theta(Db(e1)^2 - \omega \cdot e1 - k_{oxa})}$$

$$\mu = \frac{k_{ads}}{\theta(Db(e2)^2 - \omega \cdot e2 - k_{oxa})}$$

$$\rho = \frac{-k_r}{(k_r - k_{des})}$$

$$\gamma = \frac{k_{oxa} \cdot \lambda - \dfrac{k_{oxc}}{\theta}}{Db(e1)^2 - \omega \cdot e1}$$

$$\varepsilon = \frac{k_{oxa} \cdot \mu - \dfrac{k_{oxc}}{\theta}}{Db(e2)^2 - \omega \cdot e2}$$

The integration constants (B1, B2, J1, J2, F1, F2, I, H and G) were solved with the following boundary conditions:

$$\text{When } x = 0;\ C_I = C_0,\ J_{Ax=0} = -\theta\phi(DbA'_I - \omega \cdot A_I) \text{ and } J_{Sx=0} = -\theta\phi(DbS'_I - \omega \cdot S_I)$$

$$\text{When } x = L;\ \ C_I = C_{II},\ A_I = A_{II} \text{ and } S_I = S_{II}$$

$$[(1 + K_{eq})Db + Ds]C'_I - (1 + K_{eq})\omega C_I = [(1 + K_{eq})Db + Ds]C'_{II} - (1 + K_{eq})\omega C_{II}$$

$$DbA'_I - \omega A_I = DbA'_{II} - \omega A_{II} \text{ and } DbS'_I - \omega S_I = DbS'_{II} - \omega S_{II}$$

$$\text{When } x = \infty:\ \ C_{II} = C_a,\ \ A_{II} = A_{eq} \text{ and } S_{II} = S_{eq}$$

$$\text{Instantaneous reversible sorption: } [A] = \frac{K_{eq}}{\vartheta}[C]$$

REFERENCES

Aller, R. C. 1994. The sedimentary Mn cycle in Long Island Sound: Its role as intermediate oxidant and the influence of bioturbation, O_2, and C_{org} flux on diagenetic reaction balances. J. Mar. Res., *52,* 259–295.

—— 1990. Bioturbation and manganese cycling in hemipelagic sediments. Phil. Trans. Royal Soc. London, *A331,* 51–68.

Appelo, C. A. J. and D. Postma. 1999. A consistent model for surface complexation on birnessite (−MnO2) and its application to a column experiment. Geochim. Cosmochim. Acta, *63,* 3039–3048.

Archer, D. and A. Devol. 1992. Benthic oxygen fluxes on the Washington shelf and slope: A comparison of *in situ* microelectrode and chamber flux measurements. Limnol. Oceanogr., *37,* 614–629.

Bender, M. L. and D. T. Heggie. 1984. Fate of organic carbon reaching the deep-sea floor: A status report. Geochim. Cosmochim. Acta, *48,* 977–986.

Berner, R. A. 1976. Inclusion of adsorption in the modeling of early diagenesis. Earth Planet. Sci. Letts., *29,* 333–340.

Boudreau, B. P. 1997. Diagenetic Models and Their Implementation, Springer Verlag, Heidelberg, 414 pp.

—— 1998. The mean mixed depth of sediments: The wherefor and why? Limnol. Oceanogr., *43,* 524–526.

Boudreau, B. P., A. Mucci, B. Sundby, G. W. Luther and N. Silverberg. 1998. Comparative diagenesis at three sites on the Canadian continental margin. J. Mar. Res., *56,* 1259–1284.

Brewer, P. G. and D. W. Spencer. 1971. Colorimetric determination of manganese in anoxic waters. Limnol. Oceanogr., *16,* 107–110.

Bromfield, S. M. and D. J. David. 1976. Sorption and oxidation of manganous ions and the reduction of manganese oxide by cell suspensions of a manganese oxidizing bacterium. Soil Biol. Biochem., *8,* 37–43.

Bruland, K. W. 1983. Trace elements in sea-water, *in* Chemical Oceanography, J. P. Riley and R. Chester, eds., Academic Press, London, 157–220.

Burdige, D. J. and J. M. Gieskes. 1983. A pore water/solid phase diagenetic model for manganese in marine sediments. Am. J. Sci., *283,* 29–47.

Burdige, D. J. and P. E. Kepkay. 1983. Determination of bacterial oxidation rates in sediments using an *in-situ* dialysis technique, I. Laboratory studies. Geochim. Cosmochim. Acta, *47,* 1907–1916.

Burdige, D. J., S. P. Dhakar and K. H. Nealson. 1992. Effects of manganese oxide mineralogy on microbial and chemical manganese reduction. Geomicrobiol. J., *10,* 27–48.

Canfield, D. E., B. Thamdrup and J. W. Hansen. 1993. The anaerobic degradation of organic matter in Danish coastal sediments: Iron reduction, manganese reduction, and sulphate reduction. Geochim. Cosmochim. Acta, *57,* 3867–3883.

Davies, S. H. R. and J. J. Morgan. 1989. Manganese(II) oxidation kinetics on metal oxide surfaces. J. Colloid Interface Sci., *129,* 63–77.

Dhakar, S. P. and D. J. Burdige. 1996. A coupled non-linear, steady state model for early diagenetic processes in pelagic sediments. Am. J. Sci., *296,* 296–330.

Drits, V. A., E. Silvester, A. I. Gorshkov and A. Manceau. 1997. Structure of synthetic monoclinic Na-rich birnessite and hexagonal birnessite: I. Results from X-ray diffraction and selected area electron diffraction. Am. Mineral., *82,* 946–961.

Durrieu de Madron, X., P. Castaing, F. Nyffeler and T. Courp. 1999. Slope transport of suspended particulate matter on the Aquitanain margin of the Bay of Biscay. Deep-Sea Res. II, *46,* 2003–2027.

Epping, E. H. G. and W. Helder. 1997. Oxygen budgets calculated from *in situ* oxygen microprofiles for Northern Adriatic sediments. Cont. Shelf Res., *17,* 1737–1764.

Epping, E., C. Van der Zee, K. Soetaert, W. Helder. 2001. On the mineralization and burial of organic carbon in sediments of the Iberian Margin and Nazaré Canyon (NE Atlantic). Progr. Oceanogr. (in press).

Fendorf, S. E., D. L. Sparks, J. A. Franz and D. M. Camaioni. 1993. Electron paramagnetic resonance stopped-flow kinetic study of manganese(II) sorption-desorption on birnessite. Soil Sci. Soc. Am. J., *57,* 57–62.

Franklin, M. L. and J. W. Morse. 1983. The interaction of manganese(II) with the surface of calcite in dilute solutions and seawater. Mar. Chem., *12,* 241–254.

Friedl, G., B. Werhli and A. Manceau. 1997. Solid phases in the cycling of manganese in eutrophic lakes: New insights from EXAFS spectroscopy. Geochim. Cosmochim. Acta, *61,* 275–290.

Froelich, P. N., G. P. Klinkhammer, M. L. Bender, N. A. Luedtke, G. R. Heath, D. Cullen, P. Dauphin, D. Hammond, B. Hartman and V. Maynard. 1979. Early oxidation of organic matter in pelagic sediments of the eastern equatorial Atlantic: Suboxic diagenesis. Geochim. Cosmochim. Acta, *43,* 1075–1090.

Jørgensen, B. B. 1982. Mineralization of organic matter in the sea bed—The role of sulphate reduction. Nature, *296,* 643–645.

Junta, J. L. and M. F. Hochella Jr. 1994. Manganese(II) oxidation at mineral surfaces: A microscopic and spectroscopic study. Geochim. Cosmochim. Acta, *58,* 4985–4999.

Junta-Rosso, J. L., M. F. Hochella Jr. and J. D. Rimstidt. 1997. Linking microscopic and macroscopic data for heterogeneous reactions illustrated by the oxidation of manganese(II) at mineral surfaces. Geochim. Cosmochim. Acta, *61,* 149–159.

Klinkhammer, G. P. 1980. Early diagenesis in sediments from the eastern equatorial Pacific, II. Pore water metal results. Earth Planet. Sci. Letts., *49,* 81–101.

Lohse, L., W. Helder, E. H. G. Epping and W. Balzer. 1998. Recycling of organic matter along a shelf-slope transect across the N.W. European Continental Margin (Goban Spur). Progr. Oceanogr., *42,* 77–110.

Lovley, D. R. and E. J. P. Phillips. 1988. Manganese inhibition of microbial iron reduction in anaerobic sediments. Geomicrobiol. J., *6,* 145–155.

Monaco, A., X. Durrieu de Madron, O. Radakovitch, S. Heussner and J. Carbonne. 1999. Origin and variability of downward biogeochemical fluxes on the Rhone continental margin (NW Mediterranean). Deep-Sea Res. I, *46,* 1483–1511.

Morgan, J. J. and W. Stumm. 1964. Colloid-chemical properties of manganese dioxide. J. Colloid Sci., *19,* 347–359.

Morse, J. W. and G. W. Luther III. 1999. Chemical influences on trace metal-sulphide interactions in anoxic sediments. Geochim. Cosmochim. Acta, *63,* 3373–3378.

Murray, J. W. 1975. The interaction of metal ion at the manganese dioxide-solution interface. Geochim. Cosmochim. Acta, *39,* 505–519.

Myers, C. R. and K. H. Nealson. 1988a. Bacterial manganese reduction and growth with manganese oxide as the sole electron acceptor. Science, *240,* 1319–1321.

—— 1988b. Microbial reduction of manganese oxides: Interaction with iron and sulfur. Geochim. Cosmochim. Acta, *52,* 2727–2732.

Rabouille, C. and J.-F. Gaillard. 1991. Towards the EDGE: Early Diagenetic Global Exploration: A model depicting the early diagenesis of organic matter, O_2, NO_3, Mn and PO_4. Geochim. Cosmochim. Acta, *55,* 2511–2525.

Reimers, C. E., R. A. Jahnke and D. C. McCorkle. 1992. Carbon fluxes and burial rates over the continental slope and rise off central California with implications for the global carbon cycle. Global Biogeochem. Cycles, *6,* 199–224.

Sanchez-Cabeza, J. A., P. Masqué, I. Ani-Ragolta, J. Merino, M. Frignani, F. Alvisi, A. Palanques and P. Puig. 1999. Sediment accumulation rates in the southern Barcelona continental margin (NW Mediterranean Sea) derived from 210Pb and 137Cs chronology. Progr. Oceanogr., *44,* 313–332.

Schmidt, S., T. C. E. Van Weering and H. C. De Stigter. 2001a. Enhanced short-term deposition within the Nazaré Canyon, North-East Atlantic. Mar. Geol., (in press).

Schmidt, S., T. C. E. Van Weering, J.-L. Reyss and P. Van Beek. 2001b. Very recent deposition and reworking at the sea-water interface over the Iberian Margin: Seasonal and spatial trends. Progr. Oceanogr. (in press).

Slomp, C. P., J. F. P. Malschaert, L. Lohse and W. Van Raaphorst. 1997. Iron and manganese cycling in different sedimentary environments on the North Sea continental margin. Cont. Shelf Res., *17,* 1083–1117.

Soetaert, K., P. M. J. Herman and J. J. Middelburg. 1996. A model of early diagenetic processes from the shelf to abyssal depths. Geochim. Cosmochim. Acta, *60,* 1019–1040.

Soetaert, K., P. M. J. Herman, J. J. Middelburg, C. Heip, H. C. De Stigter, T. C. E. Van Weering, E. Epping and W. Helder. 1996. Modeling ^{210}Pb-derived mixing activity in ocean margin sediments: Diffusive versus nonlocal mixing. J. Mar. Res., *54,* 1207–1227.

Stone, A. T. 1987. Microbial metabolites and the reductive dissolution of manganese oxides: Oxalate and pyruvate. Geochim. Cosmochim. Acta, *51,* 919–925.

Strickland, J. D. and T. R. Parsons. 1972. A practical handbook of seawater analysis. Vol. 167, 2nd ed., Bulletin of the Fisheries Board of Canada, 311 pp.

Thamdrup, B. and D. E. Canfield. 1996. Pathways of carbon oxidation in continental margin sediments off central Chile. Limnol. Oceanogr., *41,* 1629–1650.

Thamdrup, B., R. N. Glud and J. W. Hansen. 1994. Manganese oxidation and *in situ* manganese fluxes from a coastal sediment. Geochim. Cosmochim. Acta, *58,* 2563–2570.

Ullman, W. J. and R. C. Aller. 1982. Diffusion coefficients in nearshore marine sediments. Limnol. Oceanogr., *27,* 552–556.

Van Cappellen, P. and Y. Wang. 1995. Metal cycling in surface sediments: Modeling the interplay of transport and reaction, *in* Metal Contaminated Aquatic Sediments, H. E. Allen, ed., Ann Arbor Press, 21–64.

—— 1996. Cycling of iron and manganese in surface sediments: A general theory for the coupled transport and reaction of carbon, oxygen, nitrogen, sulfur, iron and manganese. Am. J. Sci., *296,* 197–243.

Van Weering, T. C. E. and H. C. De Stigter. 1999. Recent transport and accumulation on the western Iberian Margin. OMEX II-Phase II, Second Annual Science Report, 83–92.

Van Weering, T. C. E., H. C. De Stigter, W. Boer and H. De Haas. 2001. Recent sediment transport and accumulation at the western Iberian margin. Progr. Oceanogr., (in press).

Wilson, D. E. 1980. Surface and complexation effects on the rate of Mn(II) oxidation in natural waters. Geochim. Cosmochim. Acta, *44,* 1311–1317.

Received: *19 April, 2000;* revised: *6 October, 2000.*